

# Thallium elemental and isotopic systematics in ocean island lavas

E. K. A. Brett<sup>1,\*</sup>, J. Prytulak<sup>1,2</sup>, M. Rehkämper<sup>1</sup>, S. J. Hammond<sup>3</sup>, C. Chauvel<sup>4,5</sup>, A. Stracke<sup>6</sup>, and M. Willbold<sup>7</sup>

<sup>1</sup>*Department of Earth Science and Engineering, Imperial College London, London, UK, SW7 2BP*

<sup>2</sup>*Department of Earth Science, University of Durham, Durham, UK, DH1 3LE*

<sup>3</sup>*School of Environment, Earth and Ecosystem Sciences, The Open University, Milton Keynes, UK*

<sup>4</sup>*Université de Paris, Institut de Physique du Globe de Paris, CNRS, F-75005 Paris, France*

<sup>5</sup>*ISTerre, Université Grenoble Alpes, CNRS, Grenoble, France*

<sup>6</sup>*Institut für Mineralogie, Westfälische Wilhelms-Universität Münster, Corrensstraße 24, 48149 Münster, Germany*

<sup>7</sup>*Abteilung Isotopengeologie, Universität Göttingen, Goldschmidtstraße 1, 37077 Göttingen, Germany*

\*corresponding author; email: a.brett13@imperial.ac.uk

## Abstract

The Earth's mantle exhibits marked chemical heterogeneity. We provide an examination of thallium systematics in ocean island basalts (OIB): new high-precision trace element analyses, including Tl, and Tl isotopic compositions are presented for 48 OIB spanning the entire range of observed Sr-Nd-Hf-Pb isotope ratios. All investigated OIB are characterised by ubiquitous Tl depletion requiring OIB mantle sources to have Tl concentrations as low as 0.2 ng/g, which is an order of magnitude lower than estimates for the primitive mantle and similar to Tl concentrations inferred for the depleted mantle. The low Tl concentrations inferred for OIB mantle sources are interpreted to reflect near quantitative removal of Tl during subduction and inefficient Tl recycling into the deeper mantle. If true, the Tl isotopic composition of surface materials may not be readily translated to the mantle sources of OIB.

The new OIB dataset shows a >10  $\epsilon$ -unit range in primary isotopic variation, from  $\epsilon^{205}\text{Tl} = -6.4$  to  $+6.6$ . However, the majority of samples (32 of 48) are within uncertainty of mantle values ( $\epsilon^{205}\text{Tl} = -2 \pm 1$ ), and show no co-variation with radiogenic isotopic composition. Notably, OIB with only minor Tl depletion (11 samples) have Tl isotopic compositions outside the mantle range. The Tl concentration contrast between the mantle and inputs such as sediments and altered basalt is so great that minor additions (<1% by mass) of high-Tl material will dominate the isotopic budget of a lava, with decoupling of Tl and radiogenic isotopic compositions as an expected result. Thallium isotopic compositions of OIB are therefore difficult to link directly to radiogenic isotope variations and the mantle components they may reflect. Indeed, if isotopically distinct Tl from altered oceanic crust and/or sediments were efficiently recycled into the mantle and sampled via OIB, *more* variation in the Tl isotopic composition of OIB would be expected than is observed. The markedly unsystematic primary Tl isotopic variations in OIB therefore likely reflect the residual Tl isotopic composition of subducted material, and/or Tl acquired *en route* to

the surface via shallow-level crustal assimilation.

## 1 Introduction

The majority of intraplate oceanic volcanism is the surface expression of deep-rooted thermochemical upwellings, or "mantle plumes" (e.g. Morgan, 1971; Hofmann and White, 1982; Montelli et al., 2006). Ocean island basalts (OIB) can therefore provide a window into geochemical heterogeneity of the otherwise inaccessible deep mantle (e.g. White, 2015). Zindler and Hart (1986) first proposed a classification scheme for oceanic basalts based on the observation that their radiogenic Sr-Nd-Pb isotope ratios vary systematically between a restricted number of isotopic signatures, termed mantle 'end-members' or 'components'. Decades of subsequent work has subdivided or refined the details and interpretations of the radiogenic Sr-Nd-Pb isotopic variability in oceanic basalts (e.g. Weaver, 1991; Chauvel et al., 1992; Hofmann, 1997; Workman and Hart, 2005; Willbold and Stracke, 2006). In general, the chemical variations observed in OIB can be reproduced by mixing of ambient mantle with other components, commonly identified with various recycled crustal lithologies (e.g. Hofmann and White, 1982; Weaver, 1991; Chauvel et al., 1992). Within this framework, it is suggested that the so-called HIMU (high  $\mu = {}^{238}\text{U}/{}^{204}\text{Pb}$ ) signature may represent ancient subducted oceanic crust, isolated in some cases for  $>2$  Ga. Enriched mantle (EM)-type signatures might represent incorporation of heterogeneous continental components in the form of clastic sediments or continental crust eroded at destructive plate margins (e.g. Hofmann and White, 1982; Zindler and Hart, 1986; Chauvel et al., 1992; Hofmann, 1997; Stracke et al., 2003, 2005; Workman et al., 2004; Willbold and Stracke, 2006, 2010; Stracke, 2012; Cabral et al., 2013; Hanyu et al., 2013, 2014).

Inferring mantle source compositions from the radiogenic isotope ratios observed in basalts is challenging, because sampling of the different source components via partial melting depends on a number of factors such as initial concentrations, melting behaviour, partition coefficients, extent of melt mixing, and time elapsed between fractionation events. The problem is under-constrained, resulting in an unknown extent of bias between source and melt composition (e.g. Stracke and Bourdon, 2009; Stracke, 2012). As a consequence, it is difficult to reach unambiguous interpretations of the origins and history of mantle sources.

Inferring mantle source compositions from the radiogenic isotope ratios observed in basalts is challenging, because sampling of the different source components via partial melting depends on a number of factors, such as initial concentrations, melting behaviour, partition coefficients, extent of melt mixing, and time elapsed between parent-daughter fractionation events. As a consequence, it is often difficult to reach unambiguous interpretations of the origins and history of mantle sources.

Resolving such ambiguities about the nature and origin of mantle composition and evolution on the basis of radiogenic isotopic variation observed in OIB is likely necessary to constrain global geochemical cycles and the Earth's thermal evolution. Stable isotope systematics provide useful independent constraints, as low-temperature surface environments have the potential to gener-

ate resolvable stable isotope fractionations, which might then be traced via subduction recycling into the mantle and subsequently sampled via OIB (e.g. Eiler, 2001). Analytical advances have enabled the development and application of a variety of stable isotope systems to igneous rocks, motivated in part by the potential for such systems to act as a tracer of recycled materials. Many of these advances were recently reviewed in Teng et al. (2017), for stable isotope systems from Li to U (see also Gaffney et al., 2005; Wang and Eiler, 2008; Day et al., 2009). In general, larger isotope fractionations occur in surface environments than magmatic environments, and so a logical aim is to identify the incorporation of recycled surface material by determining whether magmatic rocks carry a stable isotopic signature that is distinguishable from the mantle.

## 1.1 Thallium: a potential tracer for recycled materials

Thallium is a highly incompatible element, conventionally grouped with the alkali elements due to the similar ionic radii of  $Tl^+$  and the heavier alkali metals (e.g. Shaw, 1952; Shannon, 1976; Heinrichs et al., 1980). The relative abundance of the two stable isotopes,  $^{205}Tl$  (~70%) and  $^{203}Tl$  (~30%), is conventionally reported as  $\epsilon^{205}Tl$  relative to the NIST SRM 997 Tl isotope standard (Rehkämper and Halliday, 1999):

$$\epsilon^{205}Tl = \frac{\left(\frac{^{205}Tl}{^{203}Tl}\right)_{\text{measured}} - \left(\frac{^{205}Tl}{^{203}Tl}\right)_{\text{standard}}}{\left(\frac{^{205}Tl}{^{203}Tl}\right)_{\text{standard}}} \times 10^4$$

Before using Tl isotopic compositions to track potential mantle recycling, the effect of high-temperature igneous processes such as partial melting, metasomatism, and fractional crystallisation on Tl isotopic composition must be considered.

The effect of partial melting on stable isotope systems is often assessed by comparison of a silicate earth or ‘mantle’ value with average MORB. MORB has a Tl isotopic composition of  $\epsilon^{205}Tl = -2.0 \pm 1.0$  (2sd,  $n = 5$ ), based on fresh glass from each of the major ocean basins (Nielsen et al., 2006b, 2017b). Determining a 99 silicate Earth Tl isotopic value is more difficult. Direct measurements of Tl isotope ratios in mantle peridotites are hindered by their low concentrations (e.g. primitive mantle  $<4$  ng/g; McDonough and Sun, 1995; 4.1 ng/g; Palme and O’Neill, 2014). Currently, there is only one published measurement of unmetasomatised mantle material, a harzburgite analysed by Nielsen et al. (2015). The harzburgite has  $\epsilon^{205}Tl = -2.0 \pm 0.8$  (2sd), which is indistinguishable from MORB. Although only a single data point, the overlap with MORB can be interpreted as indicating a lack of Tl isotope fractionation during partial melting. To further investigate the mantle Tl isotopic composition and potential high temperature metasomatic processes, Fitzpayne et al. (2020) analysed mineral separates from highly metasomatised mantle xenoliths, taking advantage of the elevated concentrations of Tl in phlogopite ( $>0.2$   $\mu\text{g/g}$ ). They found a strikingly restricted range in Tl isotopic composition of  $\epsilon^{205}Tl = -2.5 \pm 1.3$  (2sd,  $n = 25$ ), which again overlaps with MORB and the single harzburgite analysis. The effect of fractional crystallisation on Tl isotopic composition was investigated by study of two co-genetic igneous suites spanning a range of  $\text{SiO}_2$  contents from Iceland and Anatahan island in the Mariana island arc (Prytulak et al., 2017). The range in Tl isotopic composition of both suites exceeds estimated external analytical precision of  $\pm 0.5$  (Hekla:  $\epsilon^{205}Tl$  from -2.2 to -0.7; Anatahan:  $\epsilon^{205}Tl$  from -2.9

to 0.0). However, the variation is not systematic with any common indices of differentiation such as MgO or SiO<sub>2</sub>. Hekla has an average  $\epsilon^{205}\text{TI} = -1.8 \pm 0.8$  (2sd, n = 14), and Anatahan has average  $\epsilon^{205}\text{TI} = -1.3 \pm 1.7$  (2sd, n = 8), which was interpreted as a lack of systematic TI isotope fractionation driven by crystal fractionation (Prytulak et al., 2017). Taken together, evidence from differentiation sequences and available mantle data implies that TI isotopic compositions are not significantly affected by partial melting, metasomatism or fractional crystallisation.

If partial melting, metasomatism and fractional crystallisation do not significantly affect TI isotopic composition, then TI isotopic variations in fresh, unaltered lavas can be interpreted as resulting from additions to their mantle source and/or assimilation *en route* to the surface.

We now consider the thallium characteristics of potential inputs. Thallium concentrations in sediments range from 100s to 10,000 of ng/g, which is 2 to 5 orders of magnitude higher than mantle abundances. Terrigenous sediments, derived from the continental crust (average TI =  $\sim 500$  ng/g e.g. Rudnick and Gao, 2003; Jenner, 2017) have TI isotopic compositions similar to MORB and loess (e.g. Nielsen et al., 2006a; Prytulak et al., 2013; Nielsen et al., 2016). Therefore, addition of terrigenous sediments to a mantle source is not expected to be readily identifiable using TI isotopes. In contrast, altered oceanic crust (AOC), altered at temperatures below 300 °C, has elevated TI concentrations ( $\sim 200$  ng/g) and light TI isotopic compositions ( $\epsilon^{205}\text{TI} \sim -20$  to  $-5$ ; Nielsen et al., 2006c, 2017b) due to hydrothermal cycling of TI through basalts, which enriches secondary minerals in light thallium isotopes (Nielsen et al., 2006a; Coggon et al., 2014). The contribution of AOC to mantle melts is therefore potentially detectable with TI isotopes. Thallium has a residence time of  $\sim 17$  kyr in seawater (Rehkämper and Nielsen, 2004), and is present only at very low concentrations ( $< 15$  pg/g; Nielsen et al., 2004) because it is readily scavenged by FeMn material. Ferromanganese materials are enriched in TI and preferentially incorporate the heavy <sup>205</sup>Tl isotope (e.g. Rehkämper et al., 2002; Peacock and Moon, 2012). Therefore, pelagic sediments and sediments rich in ferromanganese materials are enriched in TI (up to 10,000s ng/g) and have TI isotopic compositions that are often heavier than the mantle ( $\epsilon^{205}\text{TI} = 0$  to  $+15$ , per review in Nielsen et al., 2017b). Therefore, the contribution of pelagic clays and/or 147 ferromanganese materials should also be detectable with TI isotopes.

Theoretically, the contrasting TI concentrations between the mantle and surface materials, combined with distinct TI isotopic compositions, makes  $\epsilon^{205}\text{TI}$  of mantle-derived lavas extremely sensitive to contributions of some types of recycled surface materials (see e.g. illustrative calculations in Nielsen et al., 2006b; Prytulak et al., 2013). Indeed, previous work investigating subduction settings has used this framework to show that TI isotope ratios of arc lavas can be directly linked to the isotopic composition of materials subducting outboard of the associated trenches (Prytulak et al., 2013; Nielsen et al., 2015, 2016, 2017a; Shu et al., 2017, 2019). Co-variation of  $\epsilon^{205}\text{TI}$  with radiogenic isotope composition in arc lavas has been documented in some cases, where sediments dominate the trace element chemistry of the arc lavas (e.g. Aleutians; Nielsen et al., 2016). For ocean island basalts, if the presence and amount of recycled sediment and/or altered oceanic crust dominates the radiogenic isotopic composition of lavas, their TI isotopic composition might likewise co-vary with radiogenic isotopic composition. Such co-variation would only be expected if both TI and the radiogenic isotope(s) of interest are both derived from

Table 1: Summary of OIB localities with published TI concentration and isotopic composition data.

Locality	FOZO/PREMA		EMI		EM		HIMU		
	Hawai'i	Iceland	Gough	Tristan	Marquesas <sup>†</sup>	Azores	St Helena	Rurutu	Tubuai
reported [TI]	x	x			x	x	x		
reported $\epsilon^{205}\text{TI}$	x	x				x	x		
$^{87}\text{Sr}/^{86}\text{Sr}$	o	range	x	x	x	x	x	x	x
$^{143}\text{Nd}/^{144}\text{Nd}$	o	x	x	x	x	x	x	x	x
$^{176}\text{Hf}/^{177}\text{Hf}$		range	x	x	x		x		o
Pb isotopes	x	range			x	x	x	x	x
this study			x	x	x		x	x	x
key references	1*	2*,3	4,5	4,5	6	2	4,5,7	8	9

\* picrites. † Note that Marquesas lavas exhibit variable composition covering a very wide range of radiogenic isotopic compositions. x = data exists; o = partial data; range = a range is known, but samples have not been individually analysed. [1] Nielsen et al. (2006b); [2] Nielsen et al. (2017a); [3] Prytulak et al. (2017); [4] Willbold and Stracke (2006); [5] Willbold and Stracke (2010); [6] Chauvel et al. (2012); [7] Blusztajn et al. (2018); [8] Chauvel et al. (1997); [9] Chauvel et al. (1992).

the same material. In that case, if EM-type signatures reflect incorporation of recycled pelagic sediments, then isotopically heavy TI is predicted. Likewise, if the HIMU OIB signature develops via input of AOC then HIMU lavas would be expected to exhibit isotopically light TI.

Previous TI isotope studies of OIB have used the interpretive framework of isotopically heavy thallium indicating FeMn sediments and/or pelagic clays, and isotopically light thallium indicating AOC. Previous work has focussed on Hawai'i (Nielsen et al., 2006b), the Azores (Nielsen et al., 2007), Iceland (Nielsen et al., 2007; Prytulak et al., 2017), and St Helena (Blusztajn et al., 2018), documenting an overall range of  $\epsilon^{205}\text{TI} = -10$  to  $+3.9$ . This large range is mostly due to variations in rocks from Hawai'i, ascribed to the addition of FeMn sediments, and St Helena, ascribed to the addition of AOC. Thus far, no published studies have examined EM-type lavas, or HIMU lavas from localities other than St Helena. Here, we investigate EM-type lavas and expand the number of HIMU localities, to better characterize the full range of known OIB sources. All selected samples have radiogenic isotope data and show limited evidence of alteration (e.g. low loss on ignition, freshness on inspection of thin section). The 48 new analyses comprise 32 EM-type lavas from Gough, Tristan de Cunha, and the Marquesas (Fatu Hiva, Hiva Oa, Montane, Tahuata, Ua Huka) and 16 HIMU lavas from St. Helena, Rurutu, and Tubuai (Table 1). We aim to evaluate, on a global scale, the potential relationships between TI elemental abundances, TI stable isotopes, and radiogenic isotopic compositions in OIB to investigate the nature of mantle components and the efficiency of TI cycling between crust and mantle.

## 2 Methods

Sample digestions and chemical separations were carried out in the MAGIC Laboratories, Imperial College London, as described in Brett et al. (2018). Purified water (resistivity 18.2 M $\Omega$ cm from a Milli-Q system) and acids purified via sub-boiling distillation in quartz or PTFE stills were used throughout.

## 2.1 Trace element determination

While Tl concentrations can be determined during isotope ratio measurements, early studies report uncertainties of 25% (e.g. Rehkämper et al., 2002), improved to ~10% by later work (e.g. Prytulak et al., 2013) for relatively high concentration samples >20 ng/g. In contrast, the precision of Tl measurements via ICP-QQQ ("triple-quad" inductively coupled plasma mass spectrometer) is generally <4% RSD, though the uncertainty is higher for samples with lower Tl concentrations. Brett et al. (2018) provide recommendations for the Tl abundances and isotopic compositions of sixteen commonly employed reference materials based on an evaluation of existing literature and new ICP-QQQ measurements. Below, we briefly summarise the procedure employed to obtain concentration data for 39 trace elements, including Tl, at the Open University (UK) using an Agilent 8800 ICP-QQQ. For further details, please see the procedure detailed in (Brett et al., 2018).

For most samples approximately 50 mg of powder was weighed into a screw-top Savillex® PFA vial. To ensure precise and accurate determination of low Tl concentrations, ~75-100 mg of powder was weighed out for samples G6, FH-01, TH39, HV64, 74-386, and 108B. A 3:1 mixture of 29M HF and 16M HNO<sub>3</sub> was added to the vials, which were then heated to 140 °C for at least 24 hours. Samples were subsequently evaporated to *near* dryness, and dried down from 0.5-1 ml 16M HNO<sub>3</sub> at 180 °C at least three times in order to destroy insoluble fluorides formed during the initial digestion. Samples were next taken up in 2 ml 6M HCl, and refluxed at 120 °C for at least 24 hours, during which time they were ultrasonicated twice for 20 minutes, before being evaporated to complete dryness at 120 °C. 2 ml 16M HNO<sub>3</sub> and 1 ml water were then added to each sample, followed by refluxing at 140 °C for at least 24 hours. Samples were again evaporated to dryness at 140 °C, before finally being made up to 1000-fold dilution in 2% HNO<sub>3</sub>.

Sample solutions were aspirated using a quartz microflow nebuliser with an uptake rate of 0.5 ml min<sup>-1</sup>, with sensitivity on the order of 1-5 x 10<sup>7</sup> cps per µg/ml, depending on the element. Two collision/reaction gas configurations were used: no gas, for Tl and most other elements, and O<sub>2</sub>, for most Rare Earth Elements (Brett et al., 2018, see). In the no gas configuration, oxide levels, measured as CeO<sup>+</sup>/Ce<sup>+</sup>, were kept below 1%; double-charged species, measured as Ce<sup>2+</sup>/Ce<sup>+</sup>, were kept at 1.6%.

All elements except Tl were calibrated using the values provided in Eggins et al. (1997) for USGS reference materials (RMs) W-2 and DNC-1. For Tl, USGS RMs BIR-1, BHVO-2 and AGV-1 were used as calibrators, employing the values of Brett et al. (2018). Calibrator materials were run at the beginning of each measurement session. An internal solution (consisting of Be, Rh, In, Tm, Re, Bi) was added during measurement to monitor and correct instrumental drift. Drift was further monitored after every five measurements of unknown solutions with a measurement block comprising GSJ RM JB-2, 2% HNO<sub>3</sub>, and a repeated unknown sample (G-6).

## 2.2 Thallium isotope ratio determinations

Procedures for Tl separation and subsequent measurement of Tl isotopic compositions followed established protocols. Briefly, all procedures were carried out at the MAGIC Laboratories, Imperial

College London. Samples were digested via standard HF-HNO<sub>3</sub> techniques, and Tl isolated from the matrix using a 2-stage ion exchange chromatography procedure detailed in Rehkämper and Halliday (1999) and Nielsen et al. (2004), with modifications as described in Brett et al. (2018). The majority of isotope ratio measurements were performed using a Nu HR MC-ICP-MS equipped with 10<sup>11</sup> Ω resistors, as low resolution measurements using a ~100 µl/min flow rate nebuliser connected to an *Aridus*, *Aridus II* or *Nu DSN* desolvating system, with Tl solutions ranging in concentration from 2-5 ng/ml and a sensitivity of ~800 V/ppm Tl.

The limited availability of powder for some OIB samples, coupled with low Tl concentrations, required measurement of solutions with Tl concentrations of <1 ng/ml. Measurements of these low-concentration analytes on the Nu HR MC-ICP-MS are less precise than those of solutions with 2-5 ng/ml Tl. Measurements on a *Nu Plasma II MC-ICP-MS* during the later phase of the project significantly increased sensitivity compared to the Nu HR MC-ICP-MS. For Tl, sensitivity on the Nu Plasma II was routinely well in excess of 1000 V/ppm at the same measurement conditions. Otherwise, the method for isotope ratio determination on the Nu Plasma II was identical to the Nu HR, as described in Brett et al. (2018).

A secondary Tl isotope reference solution from Aldrich ('Aldrich Tl solution'), first characterised by Rehkämper and Halliday (1999), is routinely used (>2000 measurements across at least seven laboratories; Nielsen et al., 2017b) to monitor machine performance. At least two measurements of the Aldrich Tl solution were performed at the beginning and end of each session, with additional measurements performed throughout, typically after every 6 unknown samples. Additionally, a well-characterised USGS reference material (typically BCR-2, though AGV-2 and BHVO-2 were also used) was processed through the complete sample preparation procedure with every batch of 10 samples prepared for MC-ICP-MS analysis.

**Powder leaching tests.** Thallium can be concentrated in secondary clays and ferromanganese coatings. To assess possible effects of secondary, low-temperature alteration processes on Tl isotopic composition, powder leaching experiments were performed. Samples with isotopic compositions that differed from average MORB by more than 3 ε units, as determined on unleached powders, were chosen for these leaching experiments.

The leaching protocol followed the cold acid leaching of Weis and Frey (1991). Approximately 10 ml 6M HCl was added to 100-300 mg of a sample powder, and the suspension was ultrasonicated for 30 minutes. After settling for at least 30 minutes, the leachate was drawn off and discarded, and a further ~10 ml 6M HCl was added to samples, which were then ultrasonicated again for 20-30 minutes. This process was repeated until the leachate ran clear (a minimum of 3 cycles), and was then repeated a further 2 times with purified water in place of HCl. Leached powders were then evaporated, digested, separated and measured in the same manner as unleached powders.

Table 2: Key geochemical data for OIB samples analysed in this study.

Sample	MgO (wt%)*	LOI* (wt%)	Ce (µg/g)	Tl (ng/g)	Ce/Tl	ε <sup>205</sup> Tl	2sd	Dissolutions	Measurements (n)
<b>Gough (EMI)</b>									
G6	7.94	2.12	101	26	3915	0.5	2.2	2	3 (1 Nu + 2 Nu II)
G102	5.28	0.62	107	76	1402	-2.5	0.6	2	3
G117	4.52	2.49	113	39	2921	3.8	0.6	1	4
G118	12.97	1.18	73.9	49	1495	-0.6	0.5	1	2
G132	5.04	1.06	87.1	95	919	-4.6	0.5	1	3
G135	5.85	0.88	112	53	2104	-0.6	0.5	1	2
B167	3.39	3.67	107	74	1437	-3.2	0.5	1	1
<b>Tristan da Cunha (EMI)</b>									
T16	4.74	0.25	134	101	1321	-2.3	0.5	1	2
T60	12.2	-0.52	60.9	38	1600	-0.3	0.5	1	2
T64	8.91	-0.30	115	64	1796	-1.1	0.5	1	1
T122	7.28	-0.47	104	55	1888	-1.2	0.5	1	2
T497	7.61	-0.52	136	87	1559	-1.2	0.8	2	9
T557	8.00	-0.37	112	56	2006	-1.2	1.5	2	7
<i>T557 (leached)</i>						-1.6	0.9	1	1 (Nu II)
<b>Fatu Hiva, Marquesas (EM†)</b>									
FH01	10.6	0.00	110	7	16740	0.0	1.3	1	1
FH11	6.8	0.00	99.0	26	3837	-3.6	0.8	2	3
FH18	12.2	0.00	81.5	32	2554	-1.8	0.5	1	1
<b>Hiva Oa, Marquesas (EM†)</b>									
HV64	8.00	1.29	81.1	17	4649	0.7	0.5	1	1
HV76	5.14	0.32	72.7	63	1162	-0.3	0.7	1	2
<b>Montane, Marquesas (EM†)</b>									
MT04	5.63	0.01	71.6	18	3996	-3.9	1.0	3	3 (2 Nu + 1 Nu II)
MT08	5.53	0.00	82.0	25	3224	0.6	0.5	2	2
<b>Tahuata, Marquesas (EM†)</b>									
TH4	6.37	1.01	108	77	1415	-2.9	0.5	1	1
TH5	7.44	1.91	137	66	2064	-0.5	0.5	1	2
TH8	4.67	0.60	96.3	24	4045	1.0	0.5	1	1
<i>TH8 (leached)</i>						2.2	0.9	1	1 (Nu II)
TH13	6.09	-0.06	80.7	15	5482	-3.5	0.6	2	4
TH14	8.37	1.10	109	177	614	-6.4	0.5	1	4
TH18	6.40	0.28	87.6	43	2014	0.4	1.2	3	2 (1 Nu + 1 Nu II)
<i>TH18 (leached)</i>						-0.2	0.8	1	1 (Nu II)
TH31	5.6	3.00	82.1	18	4574	-1.9	1.1	2	2 (1 Nu + 1 Nu II)
TH39	9.2	0.40	81.5	18	4533	4.4	0.9	1	1
<b>Ua Huka, Marquesas (EM†)</b>									
UH53	0.38	0.76	155	235	663	-1.8	0.5	1	4
UH81	7.75	0.84	90.4	121	748	-1.9	0.5	2	5
UH89	7.2	1.63	89.8	39	2278	-3.5	0.5	1	3
UH93	9.85	0.38	72.8	97	753	-1.2	0.5	2	3
<b>St Helena (HIMU)</b>									
H28	6.64	0.13	101	26	3936	-0.9	0.5	1	5
H38	15.87	2.38	41.3	40	1043	-3.1	0.5	1	2
H64	10.97	0.72	61.7	14	4360	-0.7	0.5	1	2
H69	9.09	2.10	62.8	94	665	-3.3	0.9	2	9
<b>Rurutu, Austral-Cook (HIMU)</b>									
RRT032	6.02	1.20	47.9	45	1073	-6.4	1.3	2	4
RRT037	7.4	0.76	59.8	40	1489	6.6	0.5	1	1
<i>RRT037 (leached)</i>						4.9	0.9	1	1 (Nu II)
74-386	7.24	1.58	56.5	14	4024	-2.3	0.5	2	2
74-390	6.29	1.35	74.9	44	1709	-6.3	0.5	1	1
<i>74-390 (leached)</i>						-3.7	0.9	1	1 (Nu II)
74-396	7.89	1.06	73.9	32	2290	-3.4	0.5	1	3

continued on next page

Table 2 continued

Sample	MgO (wt%)*	LOI* (wt%)	Ce ( $\mu\text{g/g}$ )	Tl (ng/g)	Ce/Tl	$\epsilon^{205}\text{Tl}$	2sd	Dissolutions	Measurements (n)
<b>Tubuai, Austral-Cook (HIMU)</b>									
TBA9	17.9	0.25	96.4	18	5371	-2.1	1.2	1	2 (Nu II)
K109	15.5	0.3	117	19	6108	-5.9	0.5	1	1
108B	10.85	0.68	88.4	10	9069	-3.1	0.5	1	2
5433	6.2	1.42	145	31	4691	-0.3	0.5	1	2
5434	11.26	0.74	84.0	25	3393	-3.5	0.5	1	2
5435	4.85	2.58	226	50	4497	-4.8	2.4	2	3 (1 Nu + 2 Nu II)
5436	9.59	1.26	111	12	9279	-2.1	0.5	1	1

\* MgO values per Table 1 and references therein (see Electronic Annex 2b for full details).

† Marquesas lavas exhibit variable composition: at a given  $^{87}\text{Sr}/^{86}\text{Sr}$  value, lavas from the 'Ua Huka' group (Ua Huka, young Hiva Oa) have higher Nd isotopic compositions, and lavas from the 'Fatu Hiva' group (Fatu Hiva, old Hiva Oa, Montane, Tahuata) have higher  $^{206}\text{Pb}/^{204}\text{Pb}$  (see Chauvel et al., 2012; Electronic Annex 2).

2sd: where less than 3 measurements were possible, we adopt a conservative estimate based on the external reproducibility of reference materials on the instrument used. For measurements on the *Nu HR*, this is  $\pm 0.5$  based on BCR-2 measurements. For the *Nu Plasma II*, this is  $\pm 0.8$ , based on Aldrich Tl solution data, for which there are the most measurements. The average of 2 measurements is quoted if it exceeds the external reproducibility of BCR-2 on either instrument.

## 3 Results

### 3.1 Trace element concentrations

Key major and trace element concentrations for the 48 OIB samples are listed in Table 2. Thallium concentrations range from 7 to 235 ng/g. The full dataset of 39 elements is provided in Electronic Annex 1 along with results for the reference materials measured contemporaneously with the OIB samples. Trace element concentrations obtained for repeated measurement of BCR-2 and JB-2 are in good agreement with accepted values (Electronic Annex 2). For most elements, RSDs are generally  $<3\%$ ; for Tl, RSDs are  $<7\%$  for 34 samples, and  $>10\%$  for 5 samples (Fatu Hiva: FH01, FH11, FH18; St. Helena: H28; and Tubuai: K109; see Electronic Annex 2).

Many samples have existing trace element data published on the same powders (Electronic Annex 2, 3), and there is generally good agreement with previous work. We emphasize that the new data was collected with particular attention to the calibration of Tl concentration measurements, and is therefore used throughout the remainder of this work.

### 3.2 Thallium isotope ratios

The Tl isotopic composition of the 48 global OIB measured in this study are presented in Table 2, highlighting samples with isotopic compositions determined for both leached and unleached powders. Thallium isotopic compositions range from -6.4 to +6.6 and do not co-vary with Tl concentrations (Fig. 1).

The long-term intermediate precision of the Aldrich Tl solution measured on the Nu HR contemporaneously with OIB samples was  $\epsilon^{205}\text{Tl} = -0.8 \pm 0.4$  (2sd;  $n = 211$ , 14 sessions, 4 years), calculated using the average  $\epsilon^{205}\text{Tl}$  values obtained during each measurement session due to the large number of analyses. Unleached digestions of USGS reference materials AGV-2 (1), BCR-2 (10) and BHVO-2 (2) yielded  $\epsilon^{205}\text{Tl}$  values of  $-2.9 \pm 0.5$  (2sd;  $n = 3$ , 1 session),  $-2.6 \pm 0.5$  (2sd;  $n$

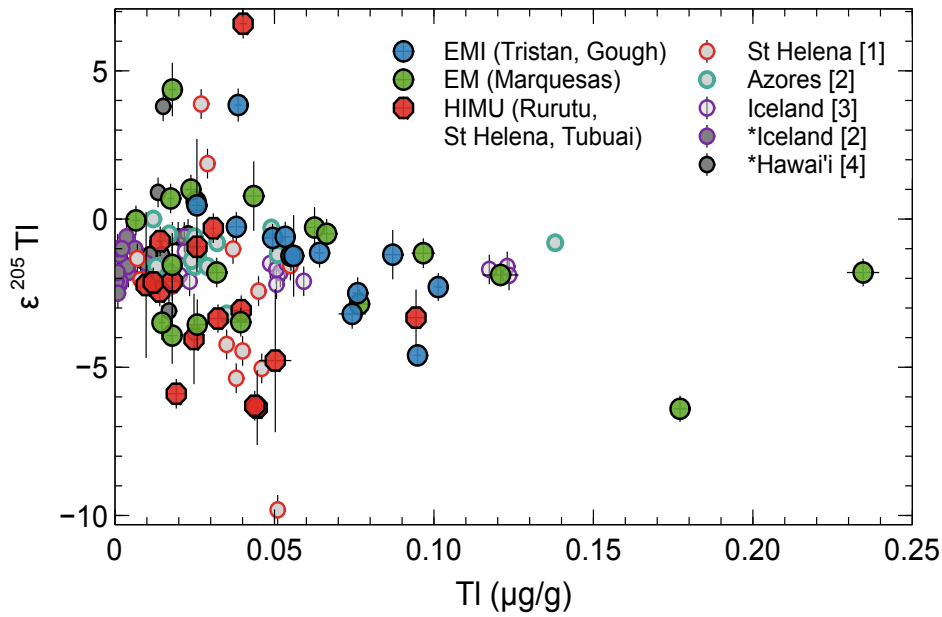


Figure 1: Plot of  $\epsilon^{205}\text{Tl}$  against Tl concentration. There is no covariation. Large symbols: this study. Other data sources: [1] Blusztajn et al. (2018); [2] Nielsen et al. (2007); [3] Prytulak et al. (2017); [4] Nielsen et al. (2006b). \* picrites.

= 21, 4 sessions), and  $-1.2 \pm 0.8$  (2sd;  $n = 3$ , 1 session) for measurements with signal intensity on mass 205 > 1 V. For measurements of BCR-2 (4 digestions) with signal intensity < 1 V,  $\epsilon^{205}\text{Tl} = -2.5 \pm 1.3$  (2sd;  $n = 21$ , 3 sessions). For both Aldrich solution and USGS reference materials, many of these determinations were first reported in Brett et al. (2018) and the values obtained are in good agreement with previous compilations (Nielsen et al., 2017b; Prytulak et al., 2017).

The average obtained for the Aldrich Tl solution on the Nu Plasma II was  $\epsilon^{205}\text{Tl} = -0.8 \pm 0.8$  (2sd;  $n = 28$ , 2 sessions, 2 months), with the higher uncertainty reflecting both the smaller number of analyses and the lower concentration of solutions. One unleached dissolution of BCR-2 yielded  $\epsilon^{205}\text{Tl} = -3.1$ , while one leached dissolution yielded  $\epsilon^{205}\text{Tl} = -2.1$ . Where only single measurements were possible, we assign the 2sd of Aldrich solution standard ( $\pm 0.8$ ) as an estimate of minimum uncertainty. Therefore, there may be a small difference between leached and unleached BCR-2. However, it is at the limits of what we can confidently interpret.

### 3.2.1 Assessing secondary effects on Tl isotope ratios

**Melt evolution.** Many stable isotope systems display isotope fractionation during fractional crystallisation of melt (e.g. Teng et al., 2017). Thallium behaviour has previously been investigated using two cogenetic suites with invariant radiogenic isotopic compositions from different tectonic settings: Hekla, Iceland, and Anatahan, Marianas (Prytulak et al., 2017). Neither suite fractionates hydrous phases, nor do they exhibit resolvable Tl isotope fractionation during differentiation. Rader et al. (2018) showed that hydrous K-rich phases such as micas can exhibit distinct Tl isotopic compositions ( $\epsilon^{205}\text{Tl}$  from -12.1 to +5.3) coupled with significant Tl enrichments (>5  $\mu\text{g/g}$ ). As such, while it is not possible to completely rule out crystallisation-induced fractionation, it is highly unlikely for the OIB studied here. With the caveat that our samples are not genetically related, there is no systematic variation of  $\epsilon^{205}\text{Tl}$  with inferred or observed phenocryst phases or

with MgO content in the current dataset (Fig. S1). We thus do not exclude any samples on this basis.

**Degassing.** Magmatic degassing can induce kinetic TI isotope fractionation (Baker et al., 2009), theoretically producing residues with heavy TI isotopic compositions and low TI concentrations relative to incompatible refractory elements in contrast with condensates with isotopically light TI, though these have yet to be reliably identified in nature. Various ratios have been employed to assess sample degassing, including Th/TI (Nielsen et al., 2007), Pb/TI (Rehkämper and Nielsen, 2004; Baker et al., 2009), Cs/TI (Prytulak et al., 2013) and Ce/TI (Nielsen et al., 2017a). The use of such ratios is challenging: Nielsen et al. (2017a) note that in arc settings, high Ce/TI ratios potentially indicative of kinetic processes are still lower than the average value for the upper mantle. In the current dataset, there is no co-variation indicative of degassing between  $\epsilon^{205}\text{TI}$  and relevant trace element concentrations or ratios for samples from individual volcanoes (not shown). This lack of chemical evidence is coupled with a lack of textural evidence for significant degassing, in that samples are thought to have been emplaced during effusive eruptions and show no significant vesicularity. Therefore, no data are rejected on this basis.

**Post-depositional effects.** In submarine lavas, both contamination (increasing the TI contents of the rocks) and alteration (decreasing the TI contents, via weathering) potentially cause resolvable differences in  $\epsilon^{205}\text{TI}$ . As little as 1  $\mu\text{g}$  of FeMn oxyhydroxide coating per gram of sample can cause an analytically resolvable shift to heavier isotope signatures, while submarine alteration may efficiently strip TI (at high temperatures) or add isotopically light TI (at low temperatures) (Nielsen et al., 2006b). Samples exhibiting very low TI concentration and  $\epsilon^{205}\text{TI}$  require scrutiny for other evidence of alteration, whereas samples with very high TI concentration and extreme  $\epsilon^{205}\text{TI}$  require scrutiny for contamination. A good example of the effects of alteration on TI concentrations and isotopic compositions is provided by the study of Blusztajn et al. (2018) on St. Helena lavas. In this case, a sample (SH-75) was excluded due to its high TI concentration (339 ng/g) combined with an isotopic composition of  $\epsilon^{205}\text{TI} = -4.06$  and visual evidence of alteration. The authors consider surficial contamination by secondary clay minerals to be the most likely explanation for these features.

All OIB lavas analysed in this study were collected subaerially, although ambiguous records mean that it is unclear if the oldest Rurutu lavas were erupted in a subaerial or submarine environment (Chauvel et al., 1997). One Rurutu lava (RRT-037) shows the highest  $\epsilon^{205}\text{TI}$  value ( $6.6 \pm 0.5$  2sd) reported for oceanic basalts thus far, warranting further assessment. However, rather than relying solely on chemical variation to identify such effects, five samples with  $\epsilon^{205}\text{TI}$  signatures significantly different from the mantle value were leached and reanalysed alongside USGS reference material BCR-2. The residues from the cold HCl leach retained 1% to 50% of the original TI, resulting in 0.05 to 1.9 ng/g total TI available for analysis ( $\sim 6$  ng/g for BCR-2), thus resulting in larger analytical errors for  $\epsilon^{205}\text{TI}$  (typically about  $\pm 1 \epsilon$ ). Notably, there is no systematic offset in  $\epsilon^{205}\text{TI}$  for the leached relative to the unleached sample powders (Table 2). This provides strong evidence that the positive and negative  $\epsilon^{205}\text{TI}$  end-members in our dataset are not due to surficial contamination by ferromanganese coatings or TI-rich secondary clay infill of fractures and cracks. Therefore, we do not exclude any samples on this basis.

Assessment of subaerial post-depositional alteration is more challenging. These processes may remove Tl from the sample without significant Tl isotope fractionation. While large fractionations do arise in low-temperature environments, strong mineralogical control is exerted by secondary sulphides in low-T hydrothermally altered oceanic crust (Coggon et al., 2014) and by birnessite in FeMn sediments (Peacock and Moon, 2012; Nielsen et al., 2013). Suspended riverine particulate matter, created through weathering, exhibits  $\epsilon^{205}\text{Tl}$  very similar to that of loess, with the oxyhydroxide fraction generally containing only minor Tl that is not isotopically distinct (Nielsen et al., 2005). Loss on ignition (LOI) is a traditional qualitative indicator of alteration, and 41 out of 48 samples have LOI less than 2 wt%. The seven samples with LOI between 2 and 4 wt% were described as showing no identifiable petrological evidence of alteration (Table 1). Therefore, no data are excluded on this basis.

## 4 Discussion

We combine our new dataset of 38 analyses with published studies to explore Tl behaviour at constructive plate margins and in intraplate settings. This results in a dataset of 93 analyses of combined elemental and isotopic determination of Tl, excluding picrites from Hawai'i and Iceland. We first revisit the relative compatibility of Tl during mantle melting, then present models of Tl behaviour during MORB and OIB melting. Finally, we examine Tl isotope systematics alongside Sr-Nd-Pb radiogenic isotopic compositions in the global OIB dataset to explore implications for cycling of Tl through the solid Earth.

### 4.1 Thallium elemental systematics

Thallium is highly incompatible during magmatic processes. Absolute Tl concentrations in OIB are thus principally determined by the extent of partial melting and fractional crystallisation. To compare the geochemistry of samples representing different degrees of melting, normalised incompatible element diagrams and ratios of trace elements with similar chemical partitioning are often employed. Quantitative assessment of how similarly two elements partition is straightforward: in a log-log plot of element concentrations, pairs of element with similar incompatibility produce a linear trend with a slope of unity (e.g. Sims and DePaolo, 1997). Such assessments are improved by taking into account the uncertainties in concentration for *both* elements (e.g. by using York regressions: York et al., 2004; Reed, 2010). In reality, however, analytical and statistical errors potentially obscure small deviations from linearity, especially between highly incompatible elements. It is therefore important to keep in mind that such relationships are at best indicative of relative compatibility contrasts. For MORB data, Nielsen et al. (2014) calculated that La, Ce, and Pb had partitioning most similar to Tl, with  $\log[\text{Tl}] - \log[\text{Ce}]$  yielding a slope of  $0.999 \pm 0.034$  (2sd,  $n = 594$ ). Results for the expanded dataset incorporating data from Yang et al. (2018) are very similar (i.e.  $0.994 \pm 0.030$  2sd; Table 3).

OIB clearly derive from heterogeneous sources. As such, there is no expectation that log-log plots would provide anything other than a very approximate indication of relative partitioning.

Table 3: Slopes obtained for York regressions (York et al., 2004) between log[Tl] and log[Element] (see text). For MORB, n = 909 except Cs, for which n = 702. For OIB, n = 48.

Element	MORB		OIB	
	slope	2sd	slope	2sd
Ce	0.994	0.030	0.102	0.122
Cs	2.608	0.036	2.033	0.571
La	1.285	0.047	0.116	0.136
Pb	0.875	0.021	1.131	0.488
Rb	3.114	0.218	1.091	0.504

Indeed, even for samples from a single location there is a marked lack of coherence in log-log diagrams of Tl versus any trace element (not shown). Of all analysed elements, the closest approach to a slope of unity with log[Tl] is achieved for log[Rb], as found by Dupuy et al. (1973) for acidic volcanic rocks (Table 3). However, the uncertainty is so high that this is not a robust result. While lower uncertainties are achieved for log[Ce] and log[La], the slope does not approximate unity. Attempting to identify elements with similar bulk partition coefficients to Tl during OIB generation using log-log plots is therefore problematic.

**Normalised incompatible element diagrams.** Thallium has been placed both between La and Ce, for low-pressure fractionation of MORB (Jenner, 2017), and between Cs and Rb (Prytulak et al., 2017, following Dupuy et al., 1973). Given the ambiguity regarding placement and the lack of compelling indications from log-log plots, we consider both compatibility orderings for the presentation of OIB data. Incompatible elements normalised to PM abundances are shown in Figure 2 (with normalisation to DM shown in Fig. S2). Notable is the marked negative Tl anomaly compared to other large-ion lithophile elements (47 of 48 samples) and REE (all samples). The La-Tl-Ce ordering produces visually similar Tl depletions to elements that are fluid-mobile during subduction processing, particularly Pb. Interestingly, the magnitude of the negative Tl anomaly co-varies with absolute Tl abundance, regardless of ordering (Fig. S3). Such co-variation would be anticipated if the ambient mantle contains negligible Tl, such that increasing Tl abundances from exotic source(s) correlate directly with less negative Tl anomalies. In this scenario, the normalising PM (and DM) Tl concentration would be overestimated.

**'Invariant' trace element ratios.** Ratios of trace elements with similar partitioning are commonly used to 'see through' the effects of magmatic evolution: where partitioning is identical, ratios should be identical in source and product. However, selecting a suitable ratio for Tl in OIB is challenging. The Cs/Tl ratio has been used, as partitioning of these two elements and their fluid mobility was assumed to be similar (e.g. Nielsen et al., 2006b; Prytulak et al., 2013, 2017). However, Cs/Tl can be affected by both degassing and possible sequestration of Tl in accessory minerals during subduction (e.g. Prytulak et al., 2013) and although Cs concentration determinations are routinely performed during ICP-MS analyses they often have relatively large errors due to the low abundance of Cs in igneous systems. The Ce/Tl ratio has also been used to assess Tl systematics in igneous settings, and has the advantage of a limited range in MORB

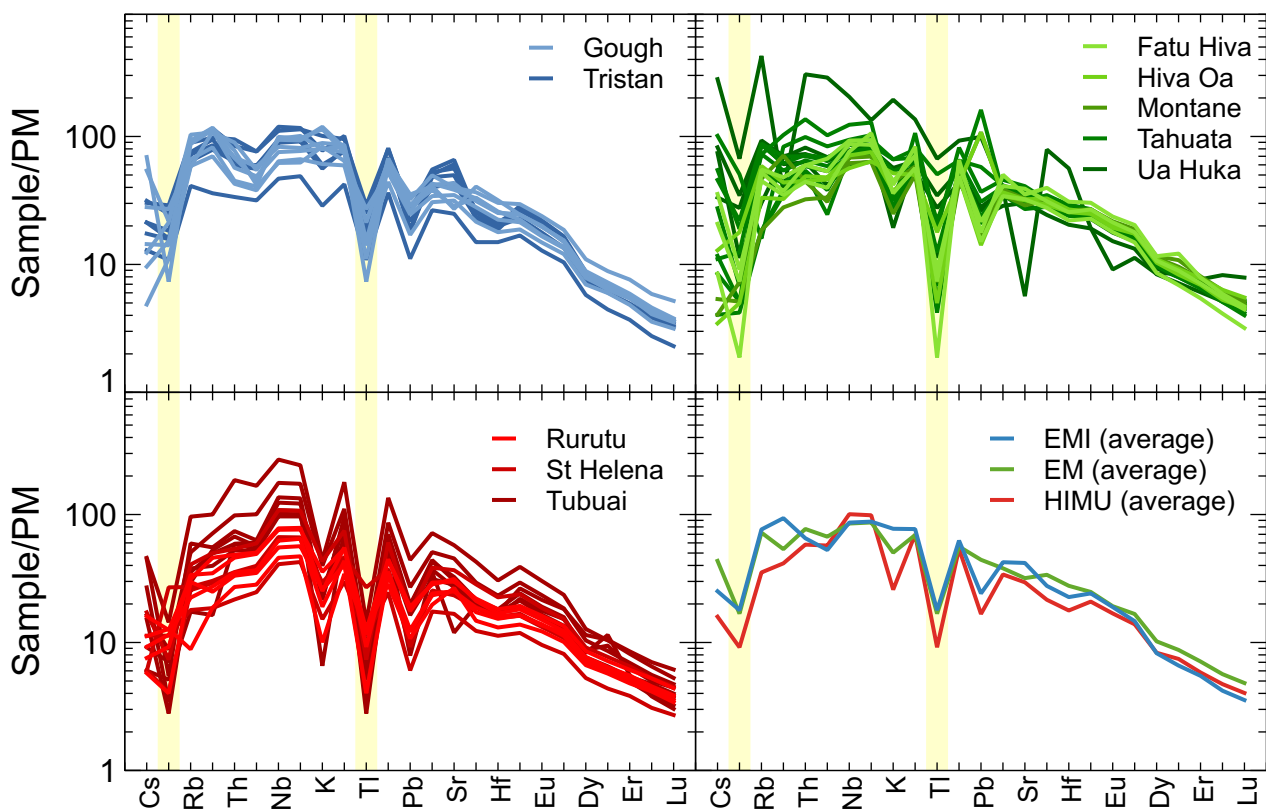


Figure 2: Primitive Mantle-normalised trace element plots. Note that Ti appears twice (highlighted), positioned both between Cs and Rb (Prytulak et al., 2017) and between La and Ce (Jenner, 2017). For almost all samples there is a clear negative Ti anomaly regardless of position, as emphasised by the averages for each end-member.

(e.g. Nielsen et al., 2014, 2017b). As Ti partitioning is clearly different between MORB and OIB regimes, no single ratio will be invariant for both tectonic settings.

In the new OIB dataset, Ce/Ti varies over an order of magnitude at a similar degree of magmatic differentiation. While absolute Ti concentrations in OIB vary with MgO content, taken as a measure of the extent of differentiation, Ce/Ti ratios do not (Fig. 3). Therefore, the range of Ce/Ti in OIB lavas likely arises from some combination of source heterogeneity and melting processes. For example, Shu et al. (2019) observed a wide range of Ce/Ti in subducted eclogites, which are geochemically similar to altered subducted oceanic crust that is thought to be a common component in OIB sources. Some authors have noted generally higher Ce/Ti ratios in OIB compared to MORB (Nielsen et al., 2014; Blusztajn et al., 2018). When examining all available data, a clear tectonic distinction between MORB, arc and OIB lavas is apparent (Fig. 4): (1) arc lavas generally exhibit the lowest Ce/Ti and highest Ti concentrations, alongside the most scattered distribution, even when filtered to exclude non-basaltic samples; (2) MORB Ce/Ti clusters around 1140, as previously discussed in Nielsen et al. (2014); and (3) global OIB form a remarkably coherent array that is clearly distinct from MORB, with overlap between the different mantle components defined by radiogenic isotopes. Similar patterns are observed for ratios of Ti with Rb, Cs, La and Pb, though with these latter ratios the different tectonic settings are less clearly distinguished (Fig. S4), motivating the further focus on Ce/Ti systematics.

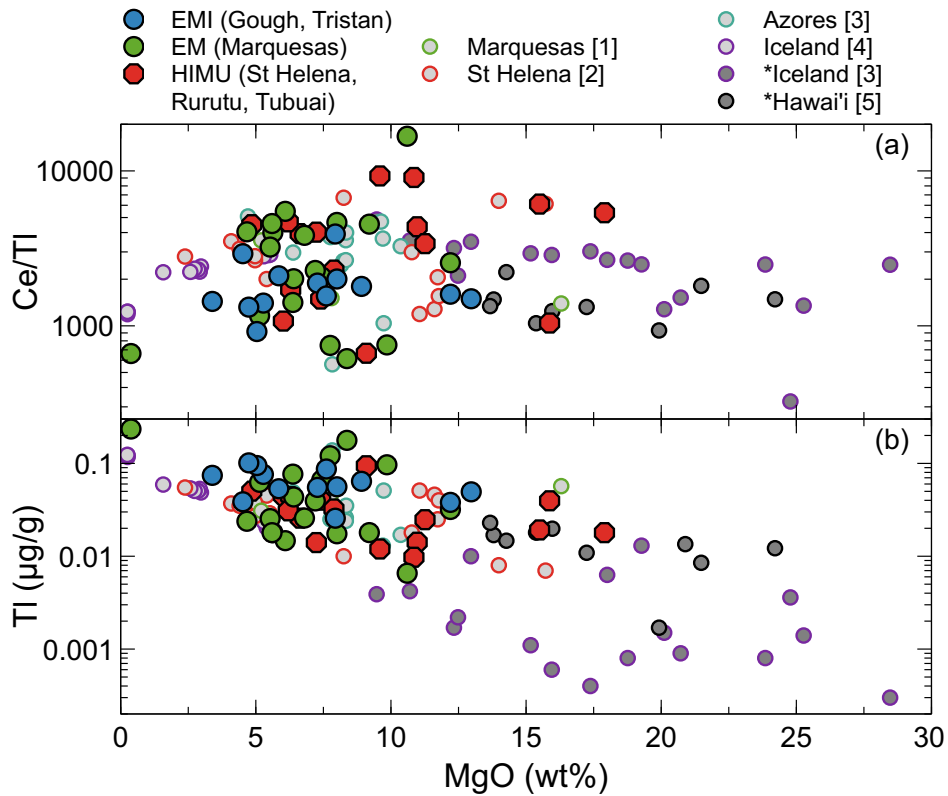


Figure 3: (a) Ce/TI and (b) TI concentrations plotted against MgO contents. Thallium is a highly incompatible element, and consequently the absolute abundance co-varies with indices of melt differentiation, such as MgO. However, Ce/TI ratios do not exhibit co-variation with melt evolution for OIB samples, indicating that Ce and TI exhibit similar incompatibility with respect to magmatic processes in the mantle. Large symbols: this study. Other data sources: [1] Chauvel et al. (2012); [2] Blusztajn et al. (2018); [3] Nielsen et al. (2007); [4] Prytulak et al. (2017); [5] Nielsen et al. (2006b). \* picrites.

## 4.2 Modelling TI variations in MORB and OIB

The systematic variation of TI versus Ce/TI in global MORB and OIB can be explored with simple melting and mixing models (Fig. 5, 6). Fractional, non-modal melting help explore the contrasting Ce/TI patterns of MORB and OIB, though simplifying assumptions must be made for several parameters (Tables 4-6). Nielsen et al. (2014) identified constraints for the majority of these parameters for MORB generation, and modelled production of the "near-uniform" Ce/TI ratio for MORB through variation of S concentrations and associated  $D_{\text{sulf/sil}}^{\text{TI}}$  values. However, subsequent findings warrant some re-evaluation of parameters.

While it is clear that TI is hosted in sulphides to some extent, recent investigations into the partitioning of TI indicates that it is less strongly chalcophile than previously assumed (e.g. Kiseeva and Wood, 2015; Wood and Kiseeva, 2015; Jenner, 2017, ; and see Appendix for detailed discussion). We therefore explored  $D_{\text{sulf/sil}}^{\text{TI}}$  values between 1 and 25 and present results for  $D_{\text{sulf/sil}}^{\text{TI}} = 10$  (e.g. Kiseeva and Wood, 2013, 2015, ; see Appendix for detailed discussion). We also consider the effects of variation in  $D_{\text{cpx/melt}}^{\text{Ce}}$  between 0.01 and 0.8, which encompasses the wide range attributed to differences in mineral chemistry (Table 5; Appendix).

**MORB.** The MORB dataset in Figure 5 combines the studies of Jenner and O'Neill (2012); Nielsen et al. (2014); Yang et al. (2018), excluding samples with MgO <6wt%, sea-mounts, back-

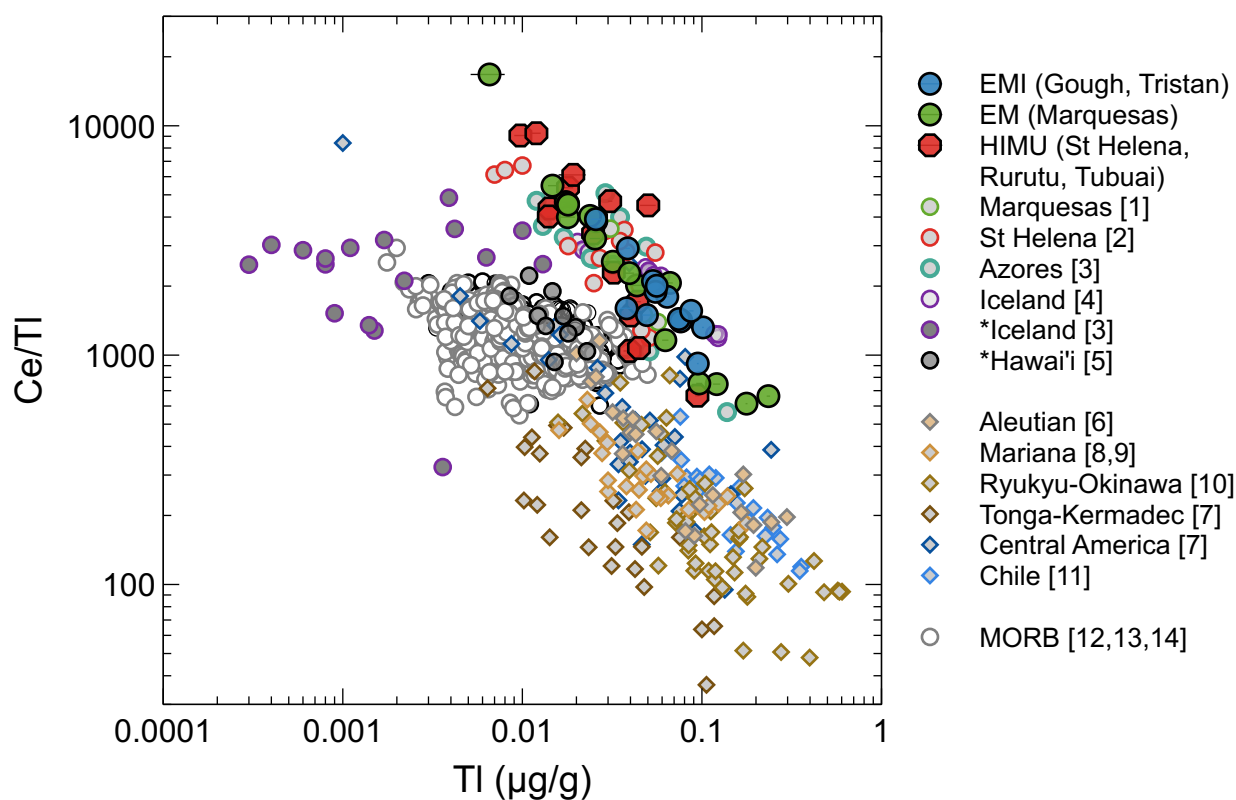


Figure 4: Plot of Ce/Tl ratios versus Tl concentrations in oceanic basalts and subduction zone volcanics. Ce/Tl trends clearly distinguish between tectonic melting regimes for fresh lavas. Note that Hawai'ian and Icelandic picritic lavas (dark gray) lie off the general OIB trend. Large symbols: this study. Other data sources (see Table 2, Electronic Annex 2): [1] Chauvel et al. (2012); [2] Blusztajn et al. (2018); [3] Nielsen et al. (2007); [4] Prytulak et al. (2017); [5] Nielsen et al. (2006b); [6] Nielsen et al. (2016); [7] Nielsen et al. (2017a); [8] Prytulak et al. (2013); [9] Prytulak et al. (2017); [10] Shu et al. (2017); [11] Cox et al. (2019); [12] Jenner and O'Neill (2012); [13] Nielsen et al. (2014); [14] Yang et al. (2018). \* picrites.

arc basins and aseismic ridges. These studies yield a combined mean MORB Ce/Tl of  $1220 \pm 570$  (2sd,  $n = 909$ ).

Fractional melting models assuming a spinel lherzolite source with variations in  $D_{\text{cpx/melt}}^{\text{Ce}}$  and initial elemental concentration are shown in Figure 5, with the fractional melting model of Nielsen et al. (2014) reproduced in Figure 5a. We explore a range of  $D_{\text{cpx/melt}}^{\text{Ce}}$  in Figure 5b, reproducing not only the average Ce/Tl value observed for MORB but also the sense of variation in the data. Compared to the model of Nielsen et al. (2014), the reduced compatibility of Tl in sulphides means that the model is less sensitive to the S concentration of the upper mantle. Considering only variations in the bulk partitioning of Ce, over 80% of MORB samples can be explained with a range of  $D_{\text{cpx/melt}}^{\text{Ce}}$  up to  $\sim 0.35$ . Furthermore, about 50% of MORB samples are explained by  $D_{\text{cpx/melt}}^{\text{Ce}} \leq 0.2$ , while fewer than 2% of MORB samples require  $D_{\text{cpx/melt}}^{\text{Ce}} \geq 0.8$ .

We also present the effects of variation in initial Tl and Ce concentration on our melting model (Fig. 5c, 5d; Appendix), with  $D_{\text{cpx/melt}}^{\text{Ce}} = 0.1$  (equivalent to bulk  $D^{\text{Ce}} = 0.015$ , i.e. the average value for peridotite melting calculated by Stracke and Bourdon, 2009). Again, variation in either of these parameters can account for both the average Ce/Tl ratio in MORB and the sense of the observed variation.

Table 4: Modal mineralogy and melt reaction coefficients used in modelling.

Mineral	spinel lherzolite (MORB)		garnet lherzolite (OIB)	
	vol proportion (%) <sup>1</sup>	melting coefficient <sup>2</sup>	vol proportion (%) <sup>3</sup>	melting coefficient <sup>3</sup>
olivine	0.57	-0.2	0.55	0.08
clinopyroxene	0.13	0.8	0.25	0.81
orthopyroxene	0.28	0.32	0.15	-0.19
spinel	0.02	0.08	-	-
garnet	-	-	0.05	0.3
sulphide	variable	SCSS*	variable	SCSS

\* Sulphur concentration at sulphide saturation (see text). [1] Workman and Hart (2005); [2] Baker and Stolper (1994) and Wasylenki et al. (2003), as modified by Nielsen et al. (2014); [3] Elliot et al. (2007).

The models thus highlight two main points:

1. As previously noted, MORB Ce/Tl exhibits some variation with Tl concentration that exceeds measurement uncertainties (Nielsen et al., 2014). We suggest that Ce/Tl variations in MORB can be explained through a combination of melting effects, a range of  $D_{\text{cpx/melt}}^{\text{Ce}}$  associated with variations in the mineral composition of clinopyroxene, and variations in source concentrations of Tl and Ce. Notably, this model does not require that bulk partition coefficients for Ce and Tl be approximately equal, and is nonetheless able to satisfy the constraint that a log-log concentration plot should exhibit a slope close to unity given the observed maximum concentration of Tl in MORB.
2. Regardless of the chosen value of  $D_{\text{cpx/melt}}^{\text{Ce}}$ , a model incorporating lower compatibility of Tl in sulphides than previously assumed yields a best fit for a  $\text{Tl}_{\text{DM}}$  abundance of 0.27 ng/g. This value is calculated assuming (i) that samples with the lowest Tl concentrations on average represent the highest degree of melting, i.e. the closest approach to the DM Ce/Tl ratio, and (ii) an average  $\text{Ce}_{\text{DM}}$  of 0.55  $\mu\text{g/g}$  (Workman and Hart, 2005). Our proposed  $\text{Tl}_{\text{DM}}$  is considerably lower than the estimate of Salters and Stracke (2004) of 0.38 ng/g, and much lower than that of Nielsen et al. (2014) of 0.48 ng/g.

**OIB.** Fractional melting models assuming either a PM or a DM source (Table 4) with up to 15% melting are shown in Figure 6a. It is immediately apparent that partial melting alone cannot produce the observed OIB Ce/Tl array from a PM or DM source, even for extreme values of  $D_{\text{cpx/melt}}^{\text{Ce}}$ . The systematics in a plot of Tl/Ce versus Tl (Minster and Allègre, 1978, ; Fig. S5) emphasise that the observed range exceeds that which can be explained by partial melting and fractional crystallisation alone, consistent with longstanding radiogenic isotopic evidence for the heterogeneous and mixed nature of OIB sources. Notably, variations in S concentration or  $D_{\text{sulf/sil}}^{\text{Tl}}$  have no significant effect on model fit, but do affect the required degree of partial melting.

To explain the variation in the OIB array we first establish constraints on the mixed source compositions. In this context, solid state mixing is assumed, rather than mixing of partial melts of

Table 5: Parameters used in models of MORB and OIB melting.

Variable	Symbol	MORB (Nielsen et al., 2014)		MORB		OIB	
		Value range	References	Value range	References	Value range	References
<i>Melting</i>							
melt fraction	F	0-16%	-	0-16%	- 0-18%	-	-
melt increment		0.01%	-	0.1%	-	0.1%	-
mean pressure		1.5 GPa	-	1.5 GPa	-	3 GPa	-
mean T		1350 °C	-	1350 °C	-	1445 °C	-
FeO in melt		~10%	8	~10%	8	~10%	sample data
SCSS		1200 µg/g	9-11	1200 µg/g	9-11	1200 µg/g	9-11
<i>Partition coefficients</i>							
Thallium	$D_{\text{cpx/melt}}^{\text{Tl}}$	0.0006	1	0.0006	1	0.0006	1
	$D_{\text{opx/melt}}^{\text{Tl}}$	0.00045	1	0.00045	1	0.00045	1
	$D_{\text{ol/melt}}^{\text{Tl}}$	$4.5 \times 10^{-5}$	1	$4.5 \times 10^{-5}$	1	$4.5 \times 10^{-5}$	1
	$D_{\text{sp/melt}}^{\text{Tl}}$	0	1	0	1	-	-
	$D_{\text{gt/melt}}^{\text{Tl}}$	-	-	-	-	0	assumed (3)
	$D_{\text{sulf/sil}}^{\text{Tl}}$	18-100	model	1-25	model	1-25	model
	Bulk D	0.0002-0.11		0.0002-0.028		0.0002-0.0007	
Cerium	$D_{\text{cpx/melt}}^{\text{Ce}}$	0.14	2	0.01-0.8	4-7	0.01-0.8	4-7
	$D_{\text{opx/melt}}^{\text{Ce}}$	0.006	2	0.006	2	0.0026	7
	$D_{\text{ol/melt}}^{\text{Ce}}$	$4 \times 10^{-5}$	2	$4 \times 10^{-5}$	2	$4 \times 10^{-5}$	2
	$D_{\text{sp/melt}}^{\text{Ce}}$	0	assumed	0	assumed	-	-
	$D_{\text{gt/melt}}^{\text{Ce}}$	-	-	-	-	0.003	3
	$D_{\text{sulf/sil}}^{\text{Ce}}$	0	assumed	0	assumed	0	assumed
	Bulk D	0.02		0.003-0.1		0.002-0.16	

[1] Assumed identical to Rb partition coefficients of Donnelly et al. (2004); [2] McDade et al. (2003a); [3] Adam and Green (2006) were unable to determine a partition coefficient for Tl between garnet and silicate melt, but for LILE, values were very low; [4] Frey (1969); [5] Irving and Frey (1984); [6] Nagasawa et al. (1969); [7] Matsui et al. (1977); [8] Gale et al. (2013); [9] Liu et al. (2007); [10] Mavrogenes and O'Neill (1999); [11] O'Neill and Mavrogenes (2002).

distinct components. Parameters including partition coefficients and initial elemental concentrations were varied until approximate matches between model output and the observed data array for up to 15% melting were achieved (Fig. 6b). We then incorporate the assumption that OIB lavas are typically the product of 3-5% melting. In this scenario, the required source materials vary over an order of magnitude in terms of Tl concentration even within a single island (Fig. 6c, 6d). A striking feature of the model is that the majority of the array requires a source that is significantly more enriched in Ce than PM estimates, without similar enrichment in Tl. Indeed, most lavas require Tl source concentrations lower than PM estimates, and in some instances lower than DM. Of all the OIB samples analysed to date only 10 (~11%) require a source Tl concentration >3.5 ng/g, i.e. more enriched in Tl than PM. These include samples from Faial in the Azores (Nielsen et al., 2007) and Tahuata and Ua Huka in Polynesia (Chauvel et al., 2012 and this work). Notably, although lavas from individual islands require source heterogeneity in terms of Tl concentration, lavas with distinct radiogenic isotopic compositions often have overlapping Ce/Tl ranges.

The mixed source concentrations required by the OIB Ce/Tl array can be interpreted as a mantle 'background' that is extremely depleted in Tl, with addition of a material characterised by high Ce and heterogeneous Tl concentrations, broadly consistent with models of widespread addition of subducted materials to the mixed OIB source. However, prior to subduction surface materials with high Ce concentrations (e.g. FeMn sediments) also exhibit elevated Tl concentrations that greatly

Table 6: Thallium and cerium concentrations in reservoirs used in modelling.

Reservoirs	Ce ( $\mu\text{g/g}$ )	Refs	Tl (ng/g)	Refs	S ( $\mu\text{g/g}$ )*	Refs
DM	0.55	1	0.27-0.48	9, <i>model</i>	0-400	2, <i>model</i>
PM	1.675	2	3.5	2	0-400	2, <i>model</i>
Peridotites	0.020-0.39	3	0.05-3.5	3	76-360	3, 12
FeMn sediment (hydrogenetic)	700	8	90000	11	-	-
Subducted eclogites†	20 (1-210)	13	60 (2-350)	11	-	-
Subduction-processed oceanic crust	~23-75	<i>calculated</i>	~2-6	<i>calculated</i>	-	-

\* Sulphide abundance was converted to S concentration using the assumption that on average mantle sulphides are 36 wt% S, i.e. domi-

nantly FeNi sulphides. †mean (Ranges). [1] Workman and Hart (2005); [2] McDonough and Sun (1995); [3] Wang et al. (2018); [4] Sparks (1995); [5] Zuleger et al. (1996); [6] Bach et al. (1996); [7] Sun and McDonough (1989); [8] Piper (1974); [9] Nielsen et al. (2014); [10] Nielsen et al. (2006c); [11] Rehkämper et al. (2002); [12] Ding and Dasgupta (2018); [13] Shu et al. (2019).

exceed values that can be accommodated by the mixing-melting model. If subducted materials are the exotic addition controlling Ce/Tl systematics in OIB, it is necessary that the majority of Tl must be removed or otherwise lost during subduction processing, rather than being recycled into the deep mantle. A 20% addition of such 'subduction-processed oceanic crust' (Table 6) to mantle strongly depleted in Tl would produce an appropriate mixed OIB source.

Recently, Shu et al. (2019) analysed the trace element and Tl isotopic composition of a number of eclogites subducted to a maximum depth of ~90 km before being exhumed, which might represent such 'subduction-processed' oceanic crust. This sample suite has an average Ce concentration of 20  $\mu\text{g/g}$  with an average Tl concentration of 55 ng/g (Table 6). While the Ce concentration is consistent with the requirements for our proposed subduction-processed oceanic crust, the Tl concentration is an order of magnitude more than the maximum we invoke to satisfy our constraints on OIB source concentrations. However, the eclogite samples remained within the stability field of Tl-rich phengite. Phengite stability depends on K and water content, but can be stable at pressures up to 4.5 GPa and temperatures of 1050 °C (e.g. Domanik and Holloway, 1997; Schmidt et al., 2004; Hermann and Spandler, 2008), with experimental work indicating near-complete loss of phengite-hosted trace elements during subduction to 300km (Schmidt et al., 2004). Once phengite has broken down, there is no obvious phase to retain Tl and carry it deeper into the mantle.

We agree with the findings of Shu et al. (2019) that OIB Ce/Tl systematics indicate widespread incorporation of subduction-processed oceanic crust into the OIB source, which may consist of (ancient, relatively enriched) oceanic crust with variable addition of a continental crust component. The Ce/Tl systematics of OIB thus highlight *similarities*, not differences, between mantle components distinguished by their radiogenic isotopic compositions. The complete overlap between different lavas representing distinct (enriched) mantle end-members strongly implies that a high-Ce, low-Tl material such as subduction-processed oceanic crust is common to OIB sources, and that Tl is near quantitatively removed during subduction.

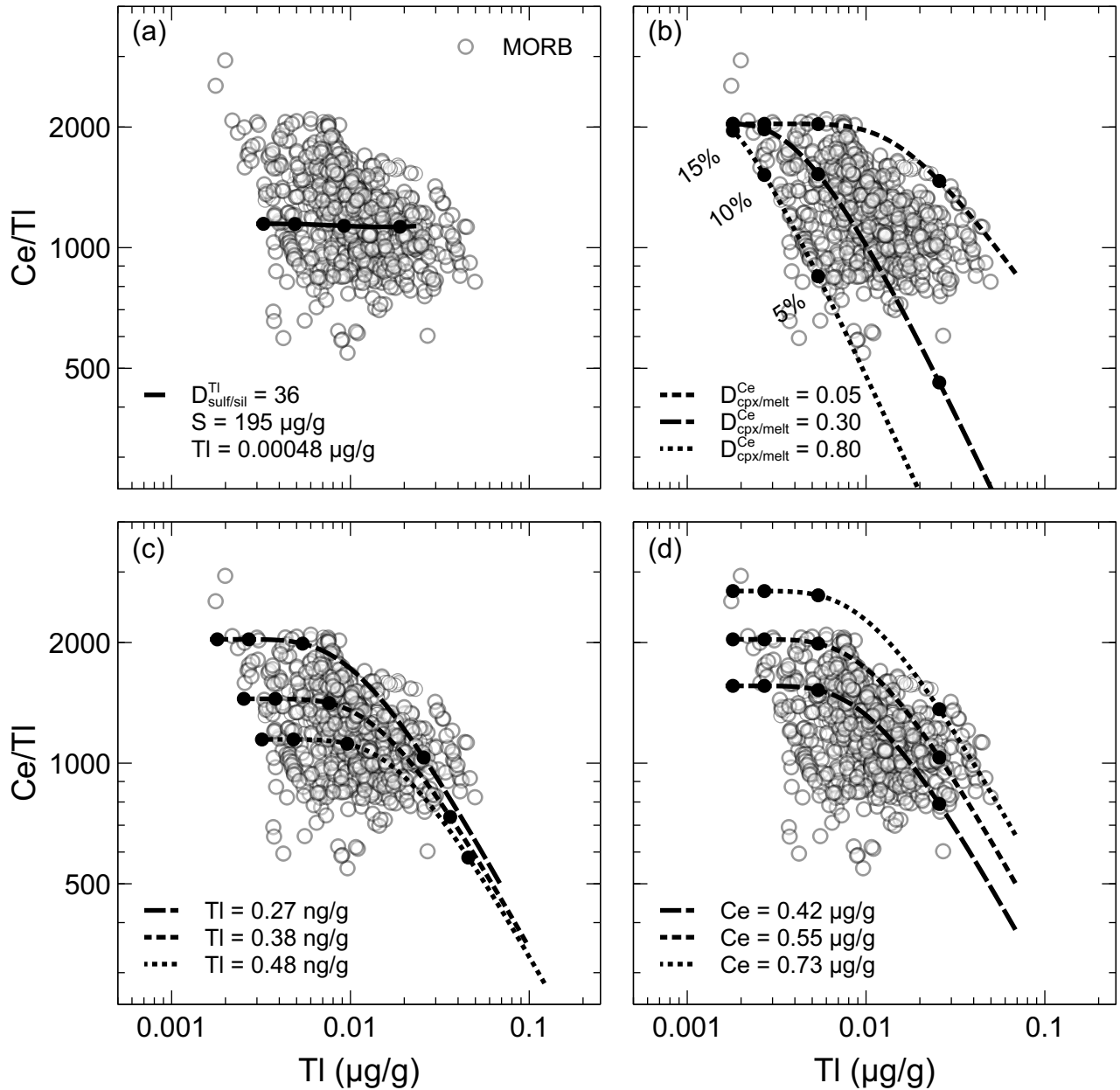


Figure 5: (a) MORB melting model of Nielsen et al. (2014), with  $Tl_{DM} = 0.48$  ng/g,  $S_{DM} = 195$   $\mu\text{g/g}$  and  $D_{sulf/sil}^{Tl} = 36$  (for other parameters see Table 5). (b) Modified MORB melting model assuming  $S_{DM} = 100$   $\mu\text{g/g}$  and  $D_{sulf/sil}^{Tl} = 10$ ; lower  $D_{sulf/sil}^{Tl}$  increases the melt percentage required to achieve any given  $Tl$ - $Ce/Tl$  data pair. In this modified model we permit variation of  $D_{cpx/melt}^{Ce}$  (see text, Table 5), reproducing both the average MORB  $Ce/Tl$  and the sense of variation. Best fit is achieved with a lower  $Tl_{DM}$  of 0.27 ng/g, implying a DM  $Ce/Tl$  of  $\sim 1800$ . (c) Modified model with variable  $Tl$  (see legend),  $Ce = 0.55$   $\mu\text{g/g}$ ,  $S = 100$   $\mu\text{g/g}$ ,  $D_{sulf/sil}^{Tl} = 10$ ,  $D_{cpx/melt}^{Ce} = 0.1$  (d) Modified melting model with  $Tl = 0.27$  ng/g, variable  $Ce$  (see legend; Workman and Hart, 2005), and other values as for subfigure (c). Symbols and data sources as in Figure 4.

### 4.3 Thallium isotopic composition of OIB

The  $Tl$  isotopic composition of the mantle is strikingly homogeneous, and no resolvable  $Tl$  isotopic fractionation is observed during partial melting or fractional crystallisation. Therefore, the significant  $Tl$  isotopic variability observed in global OIB ( $\epsilon^{205}Tl$  -10.0 to +6.6) requires the addition of isotopically distinct material to the lavas. The addition of such material can happen in the source, *en route* to the surface, and/or via subaerial/submarine alteration. We have already

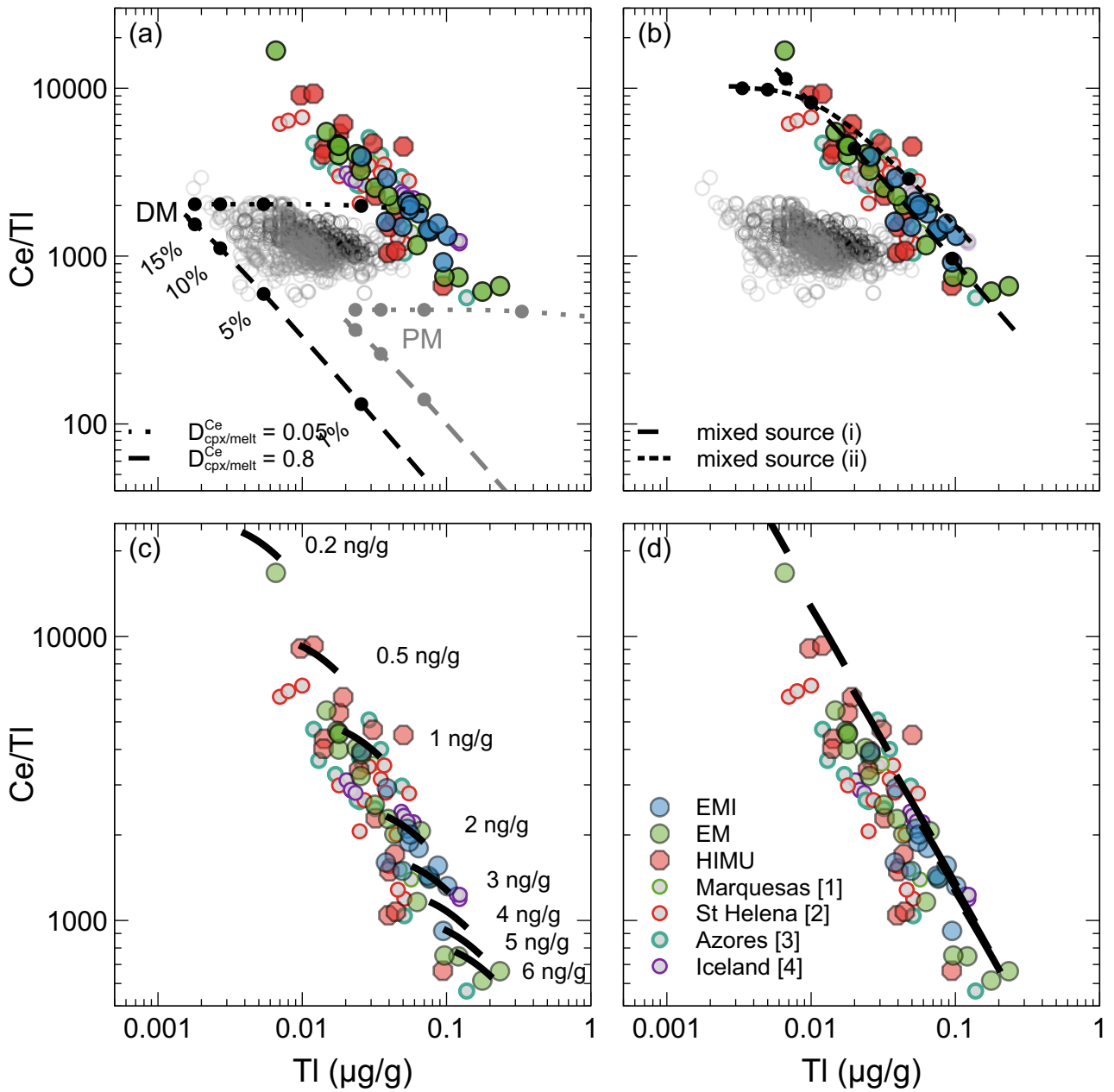


Figure 6: (a) Melting of PM (grey) and DM (black) sources (Table 6) with varying  $D_{cpx/melt}^{Ce}$ ; (b) melting of (i) a hypothetical mixed source with TI = 1 ng/g, Ce = 15 μg/g, and  $D_{cpx/melt}^{Ce} = 0.8$ ; (ii) a hypothetical mixed source with TI = 0.5 ng/g, Ce = 5 μg/g, and  $D_{cpx/melt}^{Ce} = 0.15$ . (c) 3-5% melting of a hypothetical source with Ce = 5 μg/g and  $D_{cpx/melt}^{Ce} = 0.1$ . Source TI concentration varies as indicated on figure. (d) As subfigure (c), but instead Ce = 15 μg/g and  $D_{cpx/melt}^{Ce} = 0.5$ . Large symbols: this study. Other data sources: [1] Chauvel et al. (2012); [2] Blusztajn et al. (2018); [3] Nielsen et al. (2007); [4] Prytulak et al. (2017). All displayed models assume 100 μg/g S (Ding and Dasgupta, 2018) and  $D_{sulf/sil}^{TI} = 10$ . All melting percentages as marked on subfigure (a).

argued that alteration does not play a significant role in the new data, and previous work has similarly screened and discounted altered samples.

Thallium isotopic compositions were predicted to covary with the Sr-Nd-Pb radiogenic isotopes used to classify mantle components, depending on whether AOC or recycled sediments were the primary contributor of exotic material. However, the elemental systematics of Tl in OIB appear to require highly efficient removal of Tl during subduction, which potentially weakens the link between radiogenic and Tl isotope ratios in OIB sources. Indeed, the first order observation for our global dataset is that primary Tl isotopic compositions do not co-vary with radiogenic Pb, Sr, Nd, or Hf isotopes (Fig. 7), even within the chemically diverse Marquesas island group. Although the range is large, the average  $\epsilon^{205}\text{Tl}$  for HIMU and EM-type lavas overlap within error. For HIMU  $\epsilon^{205}\text{Tl} = -2.6 \pm 6.6$  (2sd,  $n = 37$ ), and for EM  $\epsilon^{205}\text{Tl} = -1.3 \pm 4.4$  (2sd,  $n = 32$ ). The overlap remains even if the comparison is restricted to main-phase St Helena lavas and EMI-type lavas, for which  $\epsilon^{205}\text{Tl} = -3.2 \pm 3.1$  (2sd,  $n = 10$ ) and  $\epsilon^{205}\text{Tl} = -1.1 \pm 4.0$  (2sd,  $n = 13$ ), respectively. The absence of correlation between Tl isotopic compositions and Sr-Nd-Pb-Hf radiogenic isotope systems is consistent with trace element modelling that requires the mantle sources to be ubiquitously depleted in Tl, likely due to near-quantitative removal of Tl during the subduction process. Elemental parent-daughter pairs for radiogenic isotopes do not show this same level of depletion in OIB sources, and thus Tl and radiogenic Sr-Nd-Pb-Hf isotopic compositions can be easily decoupled, as noted by the first study of Tl isotopic composition in OIB (Nielsen et al., 2006b).

However, our finding that Tl isotope systematics may not be a straightforward 'fingerprint' of recycled AOC or FeMn sediment to OIB source regions is at odds with previous work. While no variation in Tl isotopic composition was found in lavas from the Azores or Iceland (Nielsen et al., 2007), incorporation of deeply subducted FeMn sediment was invoked to explain variations observed in Hawai'ian picrites (Nielsen et al., 2006b), and HIMU-type St Helena basalts have been argued to show evidence for incorporation of subducted AOC (Blusztajn et al., 2018). In the case of Hawai'i, the absence of correlation between Tl stable and Os radiogenic isotopes was noted, despite the potential for FeMn sediment contributions to control both systems, and ascribed to the very high Tl/Os ratio such sediments exhibit (Nielsen et al., 2006b).

Our new data provide a basis for re-evaluating the systematics of Tl isotopes in the HIMU mantle endmember. The isotopic criterion most commonly used to distinguish HIMU lavas is their radiogenic Pb isotopic compositions (i.e.  $^{206}\text{Pb}/^{204}\text{Pb} > 19.5$ ), which is commonly interpreted to arise from the subduction of AOC with high  $^{238}\text{U}/^{204}\text{Pb}$  ratios ('high  $\mu$ '), that was isolated in the mantle for 1-2 Ga (e.g. Hofmann and White, 1982; Zindler and Hart, 1986; Chauvel et al., 1992; Stracke et al., 2005). While acknowledging decoupling of Tl and Sr-Nd-Hf-Pb isotopes, Blusztajn et al. (2018) argue that Tl isotopic compositions that are generally lighter than those found for MORB combined with Ce/Tl variations provide evidence for the presence of a recycled upper AOC component in the St Helena source, from which up to 90% of Tl (relative to Ce) was stripped during subduction processing. Subsequent work investigated eclogites from Cabe Ortegale (Spain) and the Raspas Complex (Ecuador), thought to represent the metamorphic equivalents of altered oceanic crust (Shu et al., 2019). The eclogites have a similar range in Tl isotopic compositions as the main phase St. Helena lavas ( $\epsilon^{205}\text{Tl} \approx -5.5$  to  $-1.0$ ), and thus (Shu et al., 2019) proposed a

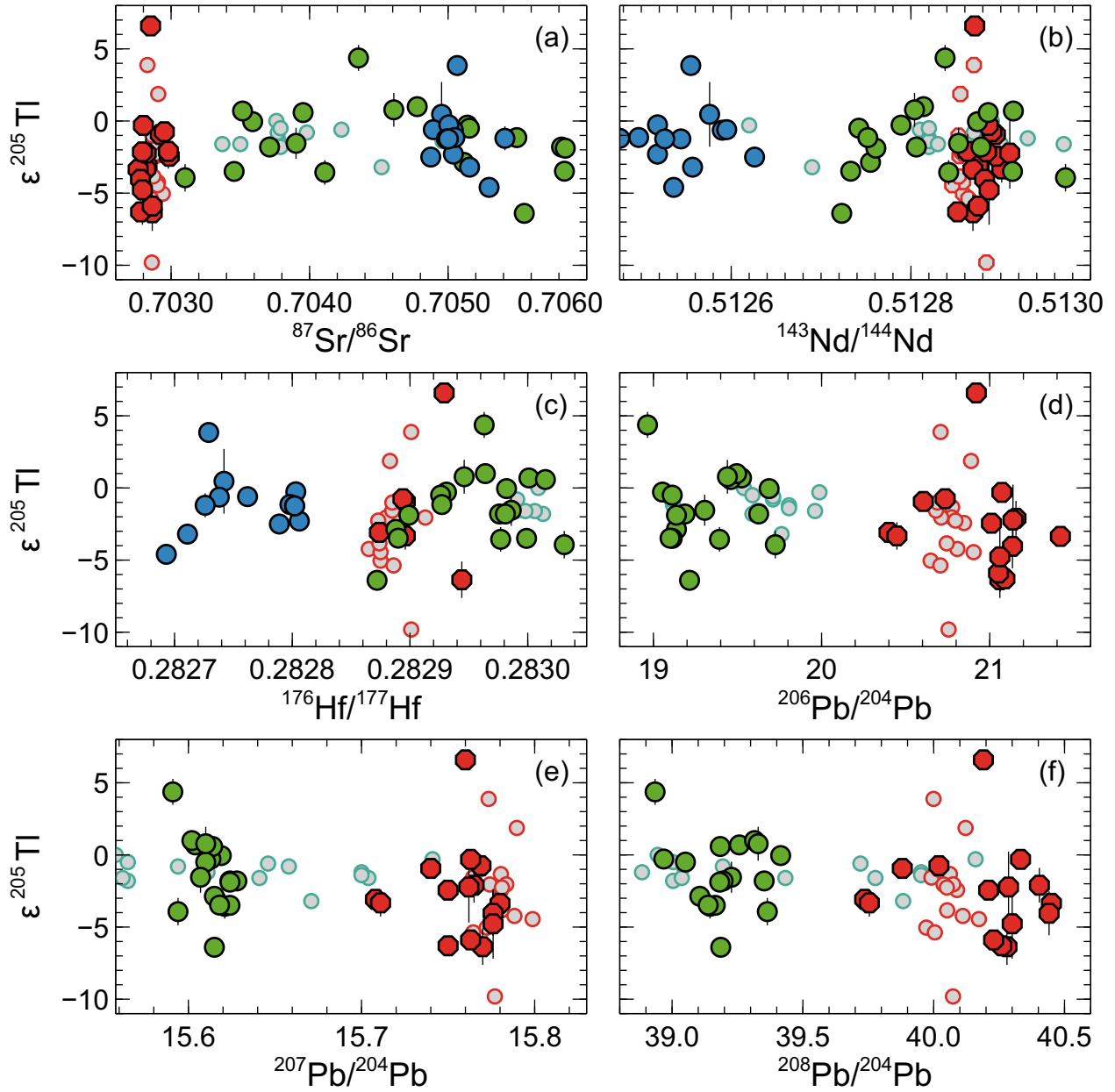


Figure 7: Plots of  $\epsilon^{205}\text{Tl}$  against (a)  $^{87}\text{Sr}/^{86}\text{Sr}$ , (b)  $^{143}\text{Nd}/^{144}\text{Nd}$ , (c)  $^{176}\text{Hf}/^{177}\text{Hf}$ , (d)  $^{206}\text{Pb}/^{204}\text{Pb}$ , (e)  $^{207}\text{Pb}/^{204}\text{Pb}$ , (f)  $^{208}\text{Pb}/^{204}\text{Pb}$ . For OIB samples, there is no co-variation of  $\epsilon^{205}\text{Tl}$  and the radiogenic isotope systems commonly used to define mantle components, with the possible exception of  $^{143}\text{Nd}/^{144}\text{Nd}$  in Icelandic picrites. Error bars are generally smaller than symbols. Symbols and data sources as in Figure 4.

genetic link between the two.

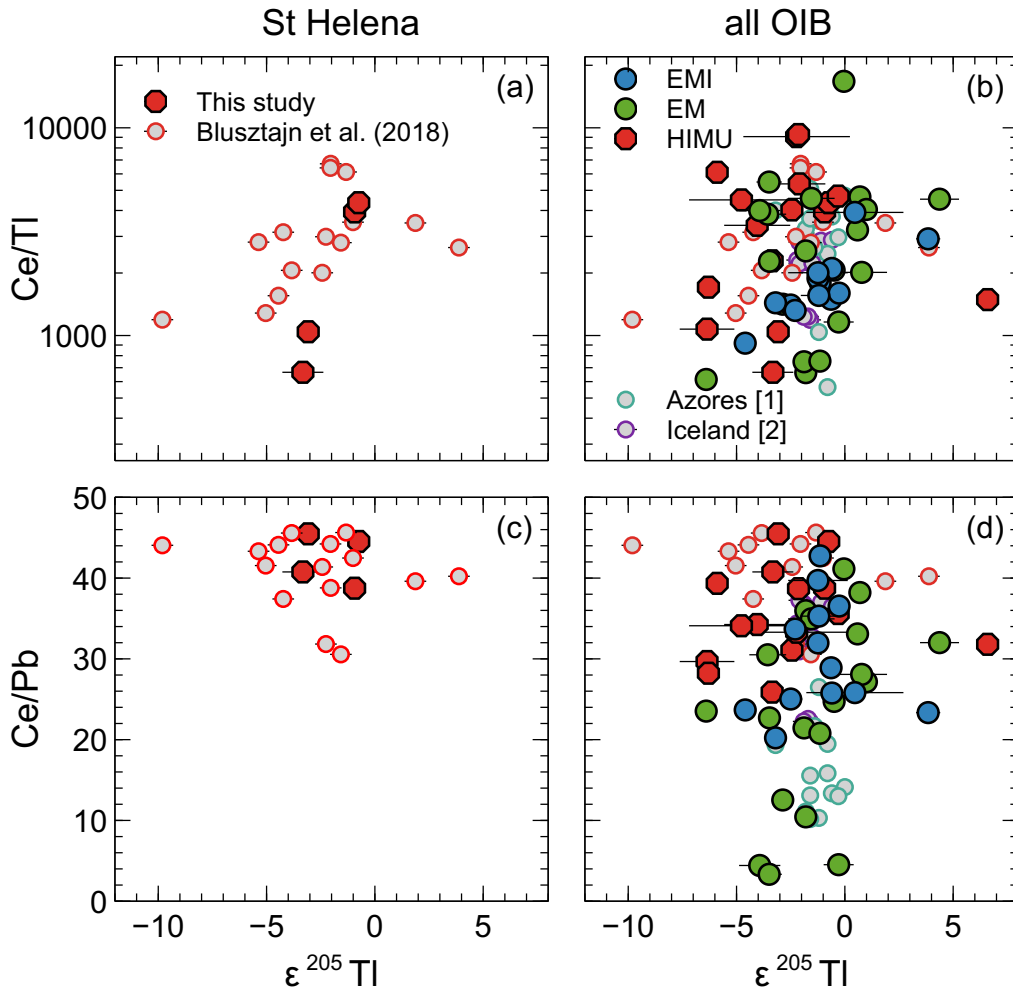


Figure 8: Plots of ratios employed to track AOC contributions to OIB source against  $\epsilon^{205}\text{Tl}$ . (a) Ce/Tl against  $\epsilon^{205}\text{Tl}$ , showing literature main-phase St Helena lavas and St Helena samples from this study, (b) Ce/Tl against  $\epsilon^{205}\text{Tl}$  for all OIB samples, (c) Ce/Pb against  $\epsilon^{205}\text{Tl}$  with the same samples as subfigure (a), (d) Ce/Pb against  $\epsilon^{205}\text{Tl}$  for all OIB samples. Blusztajn et al. (2018) argued that a sense of correlation for main-phase St Helena lavas indicated a role for subduction-processed AOC in generating the HIMU array. However, this trend is not replicated in HIMU lavas from other localities, and is not unique to HIMU-type lavas. Large symbols: this study. Other data sources: [1] Nielsen et al. (2007); [2] Prytulak et al. (2017).

This interpretation is complicated by the observation that, for the full OIB dataset (Fig. 8), the majority of HIMU samples have  $\epsilon^{205}\text{Tl}$  values that overlap with the range of results obtained for EM-type samples ( $\epsilon^{205}\text{Tl} \geq -6.5$ ; Fig. 8b, 8d). In addition, there is no convincing co-variation of  $\epsilon^{205}\text{Tl}$  with Ce/Tl and Ce/Pb for either St Helena lavas (Fig. 8a, 8c) or the complete OIB dataset, with EM-type samples again overlapping the whole range of HIMU-type lavas. While one HIMU-type lava does exhibit the lightest reported Tl isotopic composition of any OIB sampled to date ( $\epsilon^{205}\text{Tl} \approx -10$ ), the broad overlap in  $\epsilon^{205}\text{Tl}$  for HIMU- and EM-type OIB does not provide a clear distinction between different mantle end-members based on Tl isotopic compositions alone. It therefore appears that Tl isotopic compositions are decoupled not just from radiogenic isotopes and Tl concentrations, as suggested by Shu et al. (2019), but also – at least on a global scale – from incompatible trace element ratios held to be indicative of AOC contributions.

We concur with the conclusion of Blusztajn et al. (2018) that the Ce/Tl ratios of OIB appear to be broadly complementary to those found in island arc lavas. It is therefore necessary to explain how Tl isotopic systematics become (apparently) decoupled from Tl elemental systematics. Fitting our model to elemental systematics data requires highly efficient ( $\sim 99\%$ , relative to Ce) removal of Tl from heterogeneous subducting materials, with only a small proportion of subducted Tl returned to OIB source regions in the deep mantle. Therefore, the low Tl concentrations of the OIB sources produce magmas with Tl signatures that can be readily overprinted by addition of isotopically distinct material.

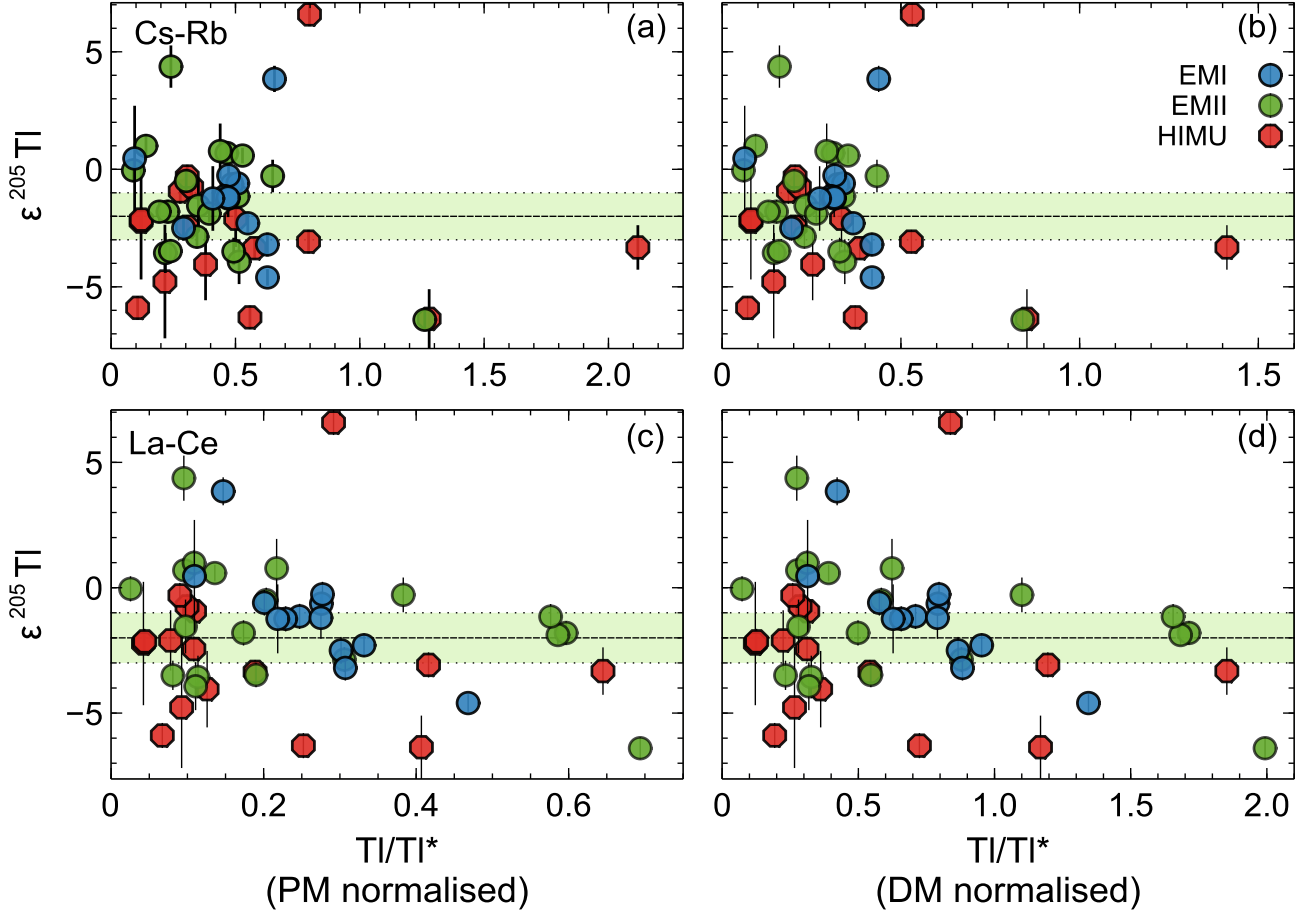


Figure 9: Plot of  $\epsilon^{205}\text{Tl}$  against  $\text{Tl}/\text{Tl}^*$  ratios ( $\text{Tl}^* = \text{Tl}/\sqrt{C_{\text{S}_N} \times R_{\text{b}_N}}$  or  $\text{Tl}/\sqrt{L_{\text{a}_N} \times C_{\text{e}_N}}$ , where N denotes concentration values normalised to PM (a,c), or DM (b,d). Relative to Cs and Rb,  $\text{Tl}/\text{Tl}^*$  values  $> 0.5$  (for both PM and DM normalisations) are associated with Tl isotopic compositions that are distinct from the mantle range (green band). Relative to La and Ce, it is less clear whether there is any association.

The notion that Tl isotopic compositions distinct from mantle values are due to the input of Tl-rich, isotopically distinct materials can be further examined via the magnitude of the negative Tl concentration anomaly observed for OIB relative to geochemically similar elements. When the magnitude of the Tl anomaly  $\text{Tl}/\text{Tl}^*$  (see caption to Figure 9) is plotted against Tl isotopic composition, samples with  $\text{Tl}/\text{Tl}^* > \sim 0.5$  (calculated relative to Cs and Rb) generally have Tl isotopic compositions that differ from the mantle (Fig. 9a, 9b). As would be expected given the decoupling of Tl and radiogenic isotopic compositions, this pattern is not restricted to or consistent within any one radiogenic isotope end-member, and some samples with  $\text{Tl}/\text{Tl}^* < \sim 0.5$  also display non-mantle values. Ruling out post-depositional isotopic effects, the question that arises is:

where does the addition of material with non-mantle Tl isotopic compositions take place? Is it during the evolution of the mantle source or *en route* to eruption?

Addition of isotopically distinct Tl to the OIB source via residual Tl from a subduction-processed slab and/or addition during ascent through the crust via assimilation of country rock, including sediments and previously-erupted and subsequently altered lavas are both reasonable processes. For example, variation in the extent and type of material assimilated during different stages of magmatism might account for the distinct average Tl isotopic compositions observed by Blusztajn et al. (2018) for St Helena early-, main-, and late-stage lavas. Given the Tl concentration contrast between magma and potential inputs, neither origin for Tl isotope variations – source heterogeneity or assimilation – would necessarily cause resolvable changes to other geochemical markers (e.g. model of Nielsen et al., 2006b; Fig. S6). Caution is therefore advisable when interpreting Tl isotopic compositions of OIB as a direct reflection of the mantle source. However, there is the potential that variable crustal assimilation of isotopically distinct Tl might be identifiable in high resolution studies of lavas from individual volcanic edifices, yielding insight into their magmatic plumbing architecture.

## 5 Conclusions

Fresh lavas from divergent, convergent and intraplate settings can be distinguished by their distinct systematics in plots of Ce/Tl ratios versus Tl concentrations. The observed patterns can be reproduced by models of fractional, non-modal melting, providing insights into the cycling of Tl through the mantle. The Ce/Tl systematics of MORB can be reproduced by the combined effects of different extents of partial melting and variations in  $D_{\text{cpx/melt}}^{\text{Ce}}$  and initial Tl and Ce concentrations, without a significant role for sulphides. In contrast, the Ce/Tl systematics of OIB cannot be generated from a primitive mantle source, but instead require a source that is markedly depleted in Tl (<1 ng/g) prior to the addition of exotic thallium. The OIB array can be generated from a depleted mantle source with addition of up to 20% subducted material from which >99% of Tl has been stripped during subduction processing. This suggests that Tl constitutes an extreme example of the behaviour of fluid-mobile elements in subduction zone settings, such that co-variations of Tl with other elements may further constrain elemental subduction zone cycling.

Thallium and radiogenic isotopic compositions are decoupled, and Tl isotopic compositions cannot be used in isolation to distinguish between continental and oceanic crust contribution to OIB source regions. The observed decoupling of Tl and radiogenic isotopic compositions most likely reflects (1) the sensitivity of Tl to small variations in the isotopic composition of residual Tl, and/or (2) the extreme Tl concentration contrast between mantle and surface materials. Despite the lack of co-variation with radiogenic isotopes, global OIB display a significant range in primary Tl isotopic compositions which must reflect addition of isotopically distinct material. However, where this Tl addition takes places remains ambiguous. The potential incorporation of Tl-rich materials at crustal levels during magma ascent is a feasible alternative interpretation to the generation of Tl isotopic variability due to incorporation of residual slab-derived Tl at mantle

depths following subduction processing.

## **6 Acknowledgements**

AB was funded by an Imperial College London Earth Science and Engineering Janet Watson departmental PhD scholarship with all analytical costs covered by start-up funds to JP. We thank Barry Coles and Katharina Kreissig for keeping the MAGIC instruments and clean labs running smoothly. CC was supported in part by ERC project SHRED (project 833632), and this is contribution 4149 of the IPGP. We appreciate the comments of Folkmar Hauff, Kevin Konrad, and four anonymous reviewers, which helped improve the manuscript.

# Appendix

## I Elemental concentrations

**MORB.** For Ce concentration, we use the values of Workman and Hart (2005) for Depleted MORB Mantle (DMM), Enriched MORB Mantle (EMM), and the average MORB source. For Tl concentration, we consider previous DM estimates along with values that provide the best fit for our model.

**OIB.** We used the values of McDonough and Sun (1995) as our initial values for PM, then varied concentrations as required to fit our model to the data.

## II Thallium partitioning

**Chalcophilia.** Nielsen et al. (2014) based their values of  $D_{\text{sulf/sil}}^{\text{Tl}}$  during MORB melting (18–100) on data from Kiseeva and Wood (2013), who reported  $D_{\text{sulf/sil}}^{\text{Tl}} = 4\text{--}24$ . However, a growing body of evidence supports the concept that ‘mixed affinity’ behaviour is exhibited by Tl, i.e. elemental behaviour cannot be described as either predominantly chalcophile or predominantly lithophile. Kiseeva and Wood (2015) report  $D_{\text{sulf/sil}}^{\text{Tl}}$  of 4–33, and note that “partitioning of most elements is a strong function of the oxygen (or FeO) content of the sulphide”, which “increases linearly with the FeO content of the silicate melt and decreases with the Ni content of the sulphide.” Wood and Kiseeva (2015) go on to state that Tl partitioning does not obey this simple model, nor one extended through consideration of additional parameters: “Despite simple and predictable partitioning behavior for many elements, several important elements (Ni, Cu, Ag, Mn, Tl) show strongly non-linear dependences of  $\log D_i$  on  $\log[\text{FeO}]$  and we were unable to assign them to any one particular category in terms of affinity for sulfide.”

Jenner (2017) calculated that for typical MORB melting  $D_{\text{sulf/sil}}^{\text{Tl}} = 7$ ; Greaney et al. (2017) observe mixed affinity behaviour during magmatic differentiation at Kilauea Iki. Wang et al. (2018) suggested that a significant proportion of the Tl contents of peridotites are hosted in interstitial late-crystallising silicate phases, finding that sulphides typically contribute <30% of the bulk rock Tl budget. These observations are consistent with poor correlation of Tl concentrations with chalcophile element concentrations in most igneous contexts (e.g. Prytulak et al., 2017).

**Silicate minerals.** Although Tl is known to be highly incompatible, partitioning of Tl between silicate minerals and melt remains poorly constrained. Nielsen et al. (2014) therefore assumed  $D_{\text{min/melt}}^{\text{Tl}}$  identical to  $D_{\text{min/melt}}^{\text{Rb}}$  due to the similarity in ionic charge and radius.  $\text{Tl}^+$  is well-known to substitute for  $\text{K}^+$  in silicate minerals (e.g. Shaw, 1952), as documented by e.g. Rader et al. (2018), and we also assume similar partitioning behaviour of Rb and Tl in silicate contexts.

## III Cerium partitioning

Although variation in mineral-melt partitioning of Ce between clinopyroxene and basaltic melt (herein  $D_{\text{cpx/melt}}^{\text{Ce}}$ ) is not required to model the MORB Ce/Tl array, it is likely that such variation does exist and does contribute to the observed pattern. The GERM database (as of June 2020)

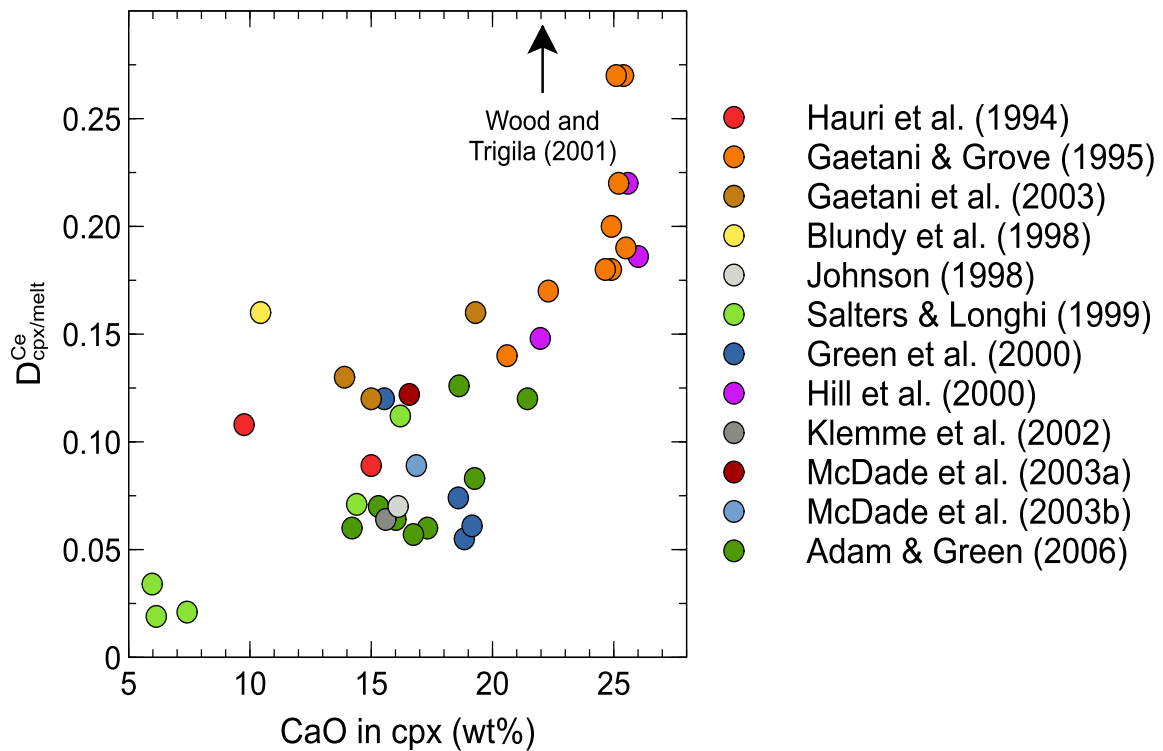


Figure A1:  $D_{\text{cpx/melt}}^{\text{Ce}}$  values versus CaO in clinopyroxene. This illustrative plot has not been corrected for pressure and temperature, or for other compositional variables including degree of hydration. With the notable exception of Green et al. (2000) and the two McDade studies, which examine melting under strongly hydrous conditions, there is a general sense of increasing Ce compatibility as CaO in cpx increases both within and between studies.

documents a total range in  $D_{\text{cpx/melt}}^{\text{Ce}}$  from 0.017 (Frey, 1969) to 0.82 (Vannucci et al., 1998), excluding the values of Nagasawa (1973), which were determined on natural samples showing signs of significant alteration (Uchimizu, 1966).  $D_{\text{cpx/melt}}^{\text{Ce}}$  is generally observed to increase with increasing Wollastonite and tetrahedrally-coordinated Al content of clinopyroxene. The data compilation of Sun and Liang (2-12) features a range of  $D_{\text{cpx/melt}}^{\text{Ce}}$  from 0.019 (Salters and Longhi, 1999) to 0.27 (Gaetani and Grove, 1995), excluding the data of Wood and Trigila (2001) determined for highly potassic melts ( $D_{\text{cpx/melt}}^{\text{Ce}}$  from 0.48 to 1.31). This information is presented graphically in Figure A1.

Johnston and Schwab (2004) additionally determined a  $D_{\text{cpx/melt}}^{\text{Ce}}$  value of 0.47 during experiments on the partial melting of peridotite (not shown). Further data for partitioning of REE in the presence of high-Ca clinopyroxenes was compiled by (Bédard, 2014), though the dataset for terrestrial basalts is limited.

While Sun and Liang (2-12) provided recommended values for  $D_{\text{cpx/melt}}^{\text{Ce}}$  during MORB melting, they note that these values are based on highly simplified thermodynamic models of clinopyroxene that may represent unrealistically restricted mineral composition ranges. We therefore explore a range of  $D_{\text{cpx/melt}}^{\text{Ce}}$  from 0.01 to 0.8 in our modelling. We do not consider 0.8 a value that is *likely* to be achieved in natural rocks, but it is informative as an end-member scenario.

## References

- J. Adam and T. Green. Trace-element partitioning between mica- and amphibole-bearing garnet lherzolite and hydrous basanitic melt: 1. Experimental results and the investigation of controls on partitioning behaviour. *Contributions to Mineralogy and Petrology*, 152:1–17, 2006. doi: 10.1007/s00410-006-0085-4.
- W. Bach, J. Erzinger, J. C. Alt, and D. A. H. Teagle. Chemistry of the lower sheeted dike complex, Hole 504B (Leg 148): influence of magmatic differentiation and hydrothermal alteration. *Proceedings of the Ocean Drilling Program, Scientific Results*, 148:39–55, 1996. doi: 10.2973/odp.proc.sr.148.114.1996.
- W. Bach, B. Peucker-Ehrenbrink, S. R. Hart, and J. S. Blusztajn. Geochemistry of hydrothermally altered oceanic crust: DSDP/ODP Hole 504B — implications for seawater–crust exchange budgets and Sr- and Pb-isotopic evolution of the mantle. *Geochemistry, Geophysics, Geosystems*, 4:8904, 2003. doi: 10.1029/2002GC000419.
- M. B. Baker and E. M. Stolper. Determining the composition of high-pressure mantle melts using diamond aggregates. *Geochimica et Cosmochimica Acta*, 58:2811–2827, 1994. doi: 10.1016/0016-7037(94)90116-3.
- R. G. A. Baker, M. Rehkämper, T. K. Hinkley, S. G. Nielsen, and J. P. Toutain. Investigation of thallium fluxes from subaerial volcanism—Implications for the present and past mass balance of thallium in the oceans. *Geochimica et Cosmochimica Acta*, 73:6340–6359, 2009. doi: 10.1016/j.gca.2009.07.014.
- J. D. Blundy, J. A. C. Robinson, and B. J. Wood. Heavy REE are compatible in clinopyroxene on the spinel lherzolite solidus. *Earth and Planetary Science Letters*, 160:493–504, 1998. doi: 10.1016/S0012-821X(98)00106-X.
- J. Blusztajn, S. G. Nielsen, H. R. Marschall, Y. Shu, C. M. Ostrander, and T. Hanyu. Thallium isotope systematics in volcanic rocks from St Helena - constraints on the origin of the HIMU reservoir. *Chemical Geology*, 476:292–301, 2018. doi: 10.1016/j.chemgeo.2017.11.025.
- E. K. A. Brett, J. Prytulak, S. J. Hammond, and M. Rehkämper. Thallium concentration and stable isotope compositions of sixteen international reference materials. *Geostandards and Geoanalytical Research*, 42:339–360, 2018. doi: 10.1111/ggr.12215.
- J. H. Bédard. Parameterizations of calcic clinopyroxene—melt trace element partition coefficients. *Geochemistry, Geophysics, Geosystems*, 15:303–336, 2014. doi: 10.1002/2013GC005112.
- R. A. Cabral, M. G. Jackson, E. F. Rose-Koga, K. T. Koga, M. J. Whitehouse, J. Farquhar, J. M. D. Day, and E. H. Hauri. Anomalous sulphur isotopes in plume lavas reveal deep mantle storage of Archaean crust. *Nature*, 496:490–493, 2013. doi: 10.1038/nature12020.
- C. Chauvel, A. W. Hofmann, and P. Vidal. HIMU-EM: The French Polynesian connection. *Earth and Planetary Science Letters*, 110:99–119, 1992. doi: 10.1016/0012-821X(92)90042-T.

- C. Chauvel, W. McDonough, G. Guille, R. Maury, and R. Duncan. Contrasting old and young volcanism in Rurutu Island, Austral chain. *Chemical Geology*, 139:125–143, 1997. doi: 10.1016/S0009-2541(97)00029-6.
- C. Chauvel, R. C. Maury, S. Blais, E. Lewin, H. Guillou, G. Guille, P. Rossi, and M.-A. Gutscher. The size of plume heterogeneities constrained by Marquesas isotopic stripes. *Geochemistry, Geophysics, Geosystems*, 13, 2012. doi: 10.1029/2012GC004123.
- R. M. Coggon, M. Rehkämper, C. Atteck, D. A. H. Teagle, J. C. Alt, and M. J. Cooper. Controls on thallium uptake during hydrothermal alteration of the upper ocean crust. *Geochimica et Cosmochimica Acta*, 144:25–42, 2014. doi: 10.1016/j.gca.2014.09.001.
- D. Cox, S. F. L. Watt, F. E. Jenner, A. R. Hastie, and S. J. Hammond. Chalcophile element processing beneath a continental arc stratovolcano. *Earth and Planetary Science Letters*, 522:1–11, 2019. doi: 10.1016/j.epsl.2019.06.017.
- J. M. D. Day, D. G. Pearson, C. Macpherson, D. Lowry, and J.-C. Carracedo. Pyroxenite-rich mantle formed by recycled oceanic lithosphere: oxygen-osmium isotope evidence from Canary Island lavas. *Geology*, 37:555–558, 2009. doi: 10.1130/G25613A.1.
- S. Ding and R. Dasgupta. Sulfur inventory of Ocean Island Basalt source regions constrained by modeling the fate of sulfide during decompression melting of a heterogeneous mantle. *Journal of Petrology*, 59:1281–1308, 2018. doi: 10.1093/petrology/egy061.
- K. J. Domanik and J. R. Holloway. The stability and composition of phengitic muscovite and associated phases from 5.5 GPa to 11 GPa: implications for deeply subducted sediments. *Geochimica et Cosmochimica Acta*, 60:4133–4150, 1997. doi: 10.1016/S0016-7037(96)00241-4.
- K. E. Donnelly, S. L. Goldstein, C. H. Langmuir, and M. Spiegelman. Origin of enriched ocean ridge basalts and implications for mantle dynamics. *Earth and Planetary Science Letters*, 226:347–366, 2004. doi: 10.1016/j.epsl.2004.07.019.
- C. Dupuy, M. Fratta, and D. M. Shaw. Partition coefficient of thallium compared with rubidium. *Earth and Planetary Science Letters*, 19:209–212, 1973. doi: 10.1016/0012-821X(73)90116-7.
- S. M. Eggins, J. D. Woodhead, L. P. J. Kinsley, G. E. Mortimer, P. Sylvester, M. T. McCulloch, J. M. Hergt, and M. R. Handler. A simple method for the precise determination of  $\geq 40$  trace elements in geological samples by ICPMS using enriched isotope internal standardisation. *Chemical Geology*, 134:311–326, 1997. doi: 10.1016/S0009-2541(96)00100-3.
- J. M. Eiler. Oxygen isotope variations of basaltic lavas and upper mantle rocks. *Reviews in Mineralogy and Geochemistry*, 43:319–364, 2001. doi: 10.2138/gsrmg.43.1.319.
- T. Elliot, J. Blichert-Toft, A. Heumann, G. Koetsier, and V. Forjaz. The origin of enriched mantle beneath São Miguel, Azores. *Geochimica et Cosmochimica Acta*, 71:219–240, 2007. doi: 10.1016/j.gca.2006.07.043.

- A. Fitzpayne, J. Prytulak, A. Giuliani, and J. Hergt. Thallium isotopic compositions of phlogopite in kimberlite-hosted MARID and PIC mantle xenoliths. *Chemical Geology*, 531:119347, 2020. doi: 10.1016/j.chemgeo.2019.119347.
- F. A. Frey. Rare earth abundances in a high-temperature peridotite intrusion. *Geochimica et Cosmochimica Acta*, 33:1429–1447, 1969. doi: 10.1016/0016-7037(69)90183-5.
- G. A. Gaetani and T. L. Grove. Partitioning of rare earth elements between clinopyroxene and silicate melt: crystal-chemical controls. *Geochimica et Cosmochimica Acta*, 59:1951–1962, 1995. doi: 10.1016/0016-7037(95)00119-0.
- G. A. Gaetani, A. Kent, T. L. Grove, I. Hutchenson, and E. M. Stolper. Mineral/melt partitioning of trace elements during hydrous peridotite partial melting. *Contributions to Mineralogy and Petrology*, 145:391–405, 2003. doi: 10.1016/0016-7037(95)00119-0.
- A. M. Gaffney, B. K. Nelson, L. Reisberg, and J. Eiler. Oxygen-osmium isotope systematics of West Maui lavas: a record of shallow level magmatic processes. *Earth and Planetary Science Letters*, 239:122–139, 2005. doi: 10.1016/j.epsl.2005.07.027.
- A. Gale, C. A. Dalton, C. H. Langmuir, Y. Su, and J.-G. Schilling. The mean composition of ocean ridge basalts. *Geochemistry, Geophysics, Geosystems*, 14, 2013. doi: 10.1029/2012GC004334.
- A. T. Greaney, R. L. Rudnick, R. T. Helz, R. M. Gaschnig, P. M. Piccoli, and R. D. Ash. The behavior of chalcophile elements during magmatic differentiation as observed in Kilauea Iki lava lake, Hawaii. *Geochimica et Cosmochimica Acta*, 210:71–96, 2017. doi: 10.1016/j.gca.2017.04.033.
- T. H. Green, J. D. Blundy, J. Adam, and G. M. Yaxley. SIMS determinations of trace element partition coefficients between garnet, clinopyroxene and hydrous basaltic liquids at 2–7.5 GPa and 1080–1200degC. *Lithos*, 53:165–187, 2000. doi: 10.1016/S0024-4937(00)00023-2.
- T. Hanyu, L. Dosso, O. Ishizuka, K. Tani, B. B. Hanan, C. Adam, S. Nakai, R. Senda, Q. Chang, and Y. Tatsumi. Geochemical diversity in submarine HIMU basalts from Austral Islands, French Polynesia. *Contributions to Mineralogy and Petrology*, 166:1285–1304, 2013. doi: 10.1007/s00410-013-0926-x.
- T. Hanyu, H. Kawabata, Y. Tatsumi, J.-I. Kimura, H. Hyodo, K. Sato, T. Miyazaki, Q. Chang, Y. Hirahara, T. Takahashi, R. Senda, and S. Nakai. Isotope evolution in the HIMU reservoir beneath St Helena: implications for the mantle recycling of U and Th. *Geochimica et Cosmochimica Acta*, 2014. doi: 10.1016/j.gca.2014.03.016.
- E. H. Hauri, T. P. Wagner, and T. L. Grove. Experimental and natural partitioning of Th-U-Pb and other trace elements between garnet, clinopyroxene and basaltic melts. *Chemical Geology*, 117:149–166, 1994. doi: 10.1016/0009-2541(94)90126-0.
- H. Heinrichs, B. Schulz-Dobrick, and K. H. Wedepohl. Terrestrial geology of Cd, Bi, Tl, Pb, Zn and Rb. *Geochimica et Cosmochimica Acta*, 44:1519–1533, 1980. doi: 10.1016/0016-7037(80)90116-7.

- J. Hermann and C. J. Spandler. Sediment melts at sub-arc depths: an experimental study. *Journal of Petrology*, 49:717–740, 2008. doi: 10.1093/petrology/egm073.
- E. Hill, B. J. Wood, and J. D. Blundy. The effect of Ca-Tschermaks component on trace element partitioning between clinopyroxene and silicate melts. *Lithos*, 53:205–217, 2000. doi: 10.1016/S0024-4937(00)00025-6.
- A. W. Hofmann. Mantle geochemistry: the message from oceanic volcanism. *Nature*, 385:219–229, 1997. doi: 10.1038/385219a0.
- A. W. Hofmann and W. M. White. Mantle plumes from ancient oceanic crust. *Earth and Planetary Science Letters*, 57:421–436, 1982. doi: 10.1016/0012-821X(82)90161-3.
- A. J. Irving and F. A. Frey. Trace element abundances in megacrysts and their host basalts: constraints on partition coefficients and megacryst genesis. *Geochimica et Cosmochimica Acta*, 48:1201–1221, 1984. doi: 10.1016/0016-7037(84)90056-5.
- F. E. Jenner. Cumulate causes for the low contents of sulfide-loving elements in the continental crust. *Nature Geoscience*, 10:524–529, 2017. doi: 10.1038/ngeo2965.
- F. E. Jenner and H. St C. O'Neill. Analysis of 60 elements in 616 ocean floor basaltic glasses. *Geochemistry, Geophysics, Geosystems*, 13, 2012. doi: 10.1029/2011GC004009.
- K. T. M. Johnson. Experimental determination of partition coefficients for rare earth and high-field-strength elements between clinopyroxene, garnet, and basaltic melt at high pressures. *Contributions to Mineralogy and Petrology*, 133:60–68, 1998. doi: 10.1007/s004100050437.
- A. D. Johnston and B. E. Schwab. Constraints on the clinopyroxene/melt partitioning of REE, Rb, Sr, Ti, Cr, Zr, and Nb during mantle melting: first insights from direct peridotite melting experiments at 1.0 GPa. *Geochimica et Cosmochimica Acta*, 68:4949–4962, 2004. doi: 10.1016/j.gca.2004.06.009.
- E. S. Kiseeva and B. J. Wood. A simple model for chalcophile element partitioning between sulphide and silicate liquids with geochemical applications. *Earth and Planetary Science Letters*, 383: 68–81, 2013. doi: 10.1016/j.epsl.2013.09.034.
- E. S. Kiseeva and B. J. Wood. The effects of composition and temperature on chalcophile and lithophile element partitioning into magmatic sulphides. *Earth and Planetary Science Letters*, 242:280–294, 2015. doi: 10.1016/j.epsl.2015.05.012.
- S. Klemme, J. D. Blundy, and B. J. Wood. Experimental constraints on major and trace element partitioning during partial melting of eclogite. *Geochimica et Cosmochimica Acta*, 71:1783–1799, 2002. doi: 10.1016/j.gca.2007.01.004.
- Y. Liu, N.-T. Samaha, and D. R. Baker. Sulfur concentration at sulfur saturation (SCSS) in magmatic silicate melts. *Geochimica et Cosmochimica Acta*, 71:1783–1799, 2007. doi: 10.1016/j.gca.2007.01.004.

- Y. Matsui, N. Onuma, H. Nagasawa, H. Higuchi, and S. Banno. Crystal structure control in trace element partitioning between crystal and magma. *Tectonics*, 100:315–324, 1977. doi: 10.3406/bulmi.1977.7155.
- J. A. Mavrogenes and H. St C. O'Neill. The relative effects of pressure, temperature and oxygen fugacity on the solubility of sulfide in mafic magmas. *Geochimica et Cosmochimica Acta*, 63: 1173–1180, 1999. doi: 10.1016/S0016-7037(98)00289-0.
- P. McDade, J. D. Blundy, and B. J. Wood. Trace element partitioning on the Tinaquillo lherzolite solidus at 1.5 GPa. *Physics of the Earth and Planetary Interiors*, 139:129–147, 2003a. doi: 10.1016/S0031-9201(03)00149-3.
- P. McDade, J. D. Blundy, and B. J. Wood. Trace element partitioning between mantle wedge peridotite and hydrous mgO-rich melt. *American Mineralogist*, 88:1825–1831, 2003b. doi: 10.2138/am-2003-11-1225.
- W. F. McDonough and S.-s. Sun. The composition of the earth. *Chemical Geology*, 120:223–253, 1995. doi: 10.1016/0009-2541(94)00140-4.
- J. F. Minster and C. Allègre. Systematic use of trace elements in igneous processes. *Contributions to Mineralogy and Petrology*, 68:37–52, 1978. doi: 10.1007/BF00375445.
- R. Montelli, G. Nolet, F. A. Dahlen, and G. Masters. A catalogue of deep mantle plumes: new results from finite-frequency tomography. *Geochemistry, Geophysics, Geosystems*, 7:Q11007, 2006. doi: 10.1029/2006GC001248.
- W. J. Morgan. Convection plumes in the lower mantle. *Nature*, 230:42–43, 1971. doi: 10.1038/230042a0.
- H. Nagasawa. Rare-earth distribution in alkali rocks from Oki-Dogo Island, Japan. *Contributions to Mineralogy and Petrology*, 39:301–308, 1973. doi: 10.1007/BF00376470.
- H. Nagasawa, H. Higuchi, and N. Onuma. Rare Earths in peridotite nodules: an explanation of the genetic relationship between basalt and peridotite nodules. *Earth and Planetary Science Letters*, 5:377–381, 1969. doi: 10.1016/S0012-821X(68)80067-6.
- S. G. Nielsen, M. Rehkämper, J. Baker, and A. N. Halliday. The precise and accurate determination of thallium isotope compositions and concentrations for water samples by MC-ICPMS. *Chemical Geology*, 204:109–124, 2004. doi: 10.1016/j.chemgeo.2003.11.006.
- S. G. Nielsen, M. Rehkämper, D. Porcelli, P. Andersson, A. N. Halliday, P. W. Swarzenski, C. Latkoczy, and D. Günther. Thallium isotope composition of the upper continental crust and rivers—an investigation of the continental sources of dissolved marine thallium. *Geochimica et Cosmochimica Acta*, 19:2007–2019, 2005. doi: 10.1016/j.gca.2004.10.025.
- S. G. Nielsen, M. Rehkämper, and A. N. Halliday. Large thallium isotopic variations in iron meteorites and evidence for lead-205 in the early solar system. *Geochimica et Cosmochimica Acta*, 70:2643–2657, 2006a. doi: 10.1016/j.gca.2006.02.012.

- S. G. Nielsen, M. Rehkämper, M. D. Norman, A. N. Halliday, and D. Harrison. Thallium isotopic evidence for ferromanganese sediments in the mantle source of Hawaiian basalts. *Nature*, 439:314–317, 2006b. doi: 10.1038/nature04450.
- S. G. Nielsen, M. Rehkämper, D. A. H. Teagle, D. A. Butterfield, J. C. Alt, and A. N. Halliday. Hydrothermal fluid fluxes calculated from the isotopic mass balance of thallium in the ocean crust. *Earth and Planetary Science Letters*, 251:120–133, 2006c. doi: 10.1016/j.epsl.2006.09.002.
- S. G. Nielsen, M. Rehkämper, A. D. Brandon, M. D. Norman, S. Turner, and S. Y. O'Reilly. Thallium isotopes in Iceland and Azores lavas – implications for the role of altered crust and mantle geochemistry. *Earth and Planetary Science Letters*, 264:332–345, 2007. doi: 10.1016/j.epsl.2007.10.008.
- S. G. Nielsen, L. E. Wasylenki, M. Rehkämper, C. L. Peacock, Z. Xue, and E. M. Moon. Towards an understanding of thallium isotope fractionation during adsorption to manganese oxides. *Geochimica et Cosmochimica Acta*, 117:252–265, 2013. doi: 10.1016/j.gca.2013.05.004.
- S. G. Nielsen, N. Shimizu, C.-T. A. Lee, and M. D. Behn. Chalcophile behaviour of thallium during MORB melting and implications for the sulfur content of the mantle. *Geochemistry, Geophysics, Geosystems*, 15, 2014. doi: 10.1002/2014GC005536.
- S. G. Nielsen, F. Klein, T. Kading, J. Blusztajn, and K. Wickham. Thallium as a tracer of fluid-rock interaction in the shallow Mariana forearc. *Earth and Planetary Science Letters*, 430:416–426, 2015. doi: 10.1016/j.epsl.2015.09.001.
- S. G. Nielsen, G. Yogodzinski, J. Prytulak, T. Plank, S. M. Kay, R. W. Kay, J. Blusztajn, J. D. Owens, M. Auro, and T. Kading. Tracking along-arc sediment inputs to the Aleutian arc using thallium isotopes. *Geochimica et Cosmochimica Acta*, 181:217–237, 2016. doi: 10.1016/j.gca.2016.03.010.
- S. G. Nielsen, J. Prytulak, J. Blusztajn, Y. Shu, M. Auro, M. Regelous, and J. Walker. Thallium isotopes as tracers of recycled materials in subduction zones: review and new data for lavas from Tonga-Kermadec and Central America. *Journal of Volcanology and Geothermal Research*, 339:23–40, 2017a. doi: 10.1016/j.jvolgeores.2017.04.024.
- S. G. Nielsen, J. Prytulak, and M. Rehkämper. Investigation and application of thallium isotope fractionation. *Reviews in Mineralogy and Geochemistry*, 82:799–850, 2017b. doi: 10.2138/rmg.2017.82.18.
- H. St C. O'Neill and J. A. Mavrogenes. The sulfide capacity and the sulfur content at sulfide saturation of silicate melts at 1400°C and 1 bar. *Journal of Petrology*, 43:1049–1087, 2002. doi: 10.1093/petrology/43.6.1049.
- H. Palme and H. St C. O'Neill. Cosmochemical estimates of mantle composition. In D. H. Heinrich and K. T. Karl, editors, *Treatise on Geochemistry (Second Edition)*, pages 1–38. Elsevier, Amsterdam, 2014. doi: 10.1016/B978-0-08-095975-7.00201-1.

- C. L. Peacock and E. M. Moon. Oxidative scavenging of thallium by birnessite: explanation for thallium enrichment and stable isotope fractionation in marine ferromanganese precipitates. *Geochimica et Cosmochimica Acta*, 84:297–313, 2012. doi: 10.1016/j.gca.2012.01.036.
- D. Z. Piper. Rare earth elements in ferromanganese nodules and other marine phases. *Geochimica et Cosmochimica Acta*, 38:1007–1022, 1974. doi: 10.1016/0016-7037(74)90002-7.
- J. Prytulak, S. G. Nielsen, T. Plank, M. Barker, and T. Elliott. Assessing the utility of thallium and thallium isotopes for tracing subduction zone inputs to the Mariana arc. *Chemical Geology*, 345: 129–149, 2013. doi: 10.1016/j.chemgeo.2013.03.003.
- J. Prytulak, E. K. A. Brett, M. Webb, M. Rehkämper, T. Plank, P. S. Savage, and J. Woodhead. Thallium elemental behavior and stable isotope fractionation during magmatic processes. *Chemical Geology*, 448:71–83, 2017. doi: 10.1016/j.chemgeo.2016.11.007.
- S. T. Rader, F. K. Mazdab, and M. D. Barton. Mineralogical thallium geochemistry and isotope variations from igneous, metamorphic, and metasomatic systems. *Geochimica et Cosmochimica Acta*, 243:42–65, 2018. doi: 10.1016/j.gca.2018.09.019.
- B. C. Reed. A spreadsheet for linear least-squares fitting with errors in both coordinates. *Physics Education*, 45:93–96, 2010. doi: 10.1088/0031-9120/45/1/011.
- M. Rehkämper and A. N. Halliday. The precise measurement of Tl isotopic compositions by MC-ICPMS: application to the analysis of geological materials and meteorites. *Geochimica et Cosmochimica Acta*, 63:935–944, 1999. doi: 10.1016/S0016-7037(98)00312-3.
- M. Rehkämper and S. G. Nielsen. The mass balance of dissolved thallium in the oceans. *Marine Chemistry*, 85:125–139, 2004. doi: 10.1016/j.marchem.2003.09.006.
- M. Rehkämper, M. Frank, J. R. Hein, D. Porcelli, A. N. Halliday, J. Ingri, and V. Liebetrau. Thallium isotope variations in seawater and hydrogenetic, diagenetic, and hydrothermal ferromanganese deposits. *Earth and Planetary Science Letters*, 197:65–81, 2002. doi: 10.1016/S0012-821X(02)00462-4.
- R. L. Rudnick and S. Gao. Composition of the continental crust. *Treatise on Geochemistry*, 3:1–64, 2003. doi: 10.1016/B0-08-043751-6/03016-4.
- V. J. M. Salters and J. Longhi. Trace element partitioning during the initial stages of melting beneath mid-ocean ridges. *Earth and Planetary Science Letters*, 166:15–30, 1999. doi: 10.1016/S0012-821X(98)00271-4.
- V. J. M. Salters and A. Stracke. Composition of the depleted mantle. *Geochemistry, Geophysics, Geosystems*, 5, 2004. doi: 10.1029/2003GC000597.
- M. W. Schmidt, D. Vielzeuf, and E. Auzanneau. Melting and dissolution of subducting crust at high pressures: the key role of white mica. *Earth and Planetary Science Letters*, 228:65–84, 2004. doi: 10.1016/j.epsl.2004.09.020.

- R. D. Shannon. Revised effective ionic radii and systematic studies of interatomic distances in halides and chalcogenides. *Acta Crystallographica*, A32:751–767, 1976. doi: 10.1107/S0567739476001551.
- D. M. Shaw. The geochemistry of thallium. *Geochimica et Cosmochimica Acta*, 2:118–154, 1952. doi: 10.1016/0016-7037(52)90003-3.
- Y. Shu, S. G. Nielsen, Z. Zeng, R. Shinjo, J. Blusztajn, X. Wang, and S. Chen. Tracing subducted sediment inputs to the Ryuku arc-Okinawa Trough system: evidence from thallium isotopes. *Geochimica et Cosmochimica Acta*, 217:462–491, 2017. doi: 10.1016/j.gca.2017.08.035.
- Y. Shu, S. G. Nielsen, H. R. Marschall, T. John, J. Blusztajn, and M. Auro. Closing the loop: subducted eclogites match thallium isotope compositions of ocean island basalts. *Geochimica et Cosmochimica Acta*, 250:130–148, 2019. doi: 10.1016/j.gca.2019.02.004.
- K. W. W. Sims and D. J. DePaolo. Inferences about mantle magma sources from incompatible element concentration ratios in oceanic basalts. *Geochimica et Cosmochimica Acta*, 61:765–784, 1997. doi: 10.1016/S0016-7037(96)00372-9.
- J. W. Sparks. Geochemistry of the lower sheeted dyke complex, Hole 504B, Leg 140. *Proceedings of the Ocean Drilling Program Scientific Results*, 137:81–97, 1995. ISSN 0884-5891.
- H. Staudigel, G. Davies, S. R. Hart, K. M. Marchant, and B. M. Smith. Large scale Sr, Nd, and O isotopic anatomy of altered oceanic crust at DSDP/ODP sites 417/418. *Earth and Planetary Science Letters*, 130:169–185, 1995. doi: 10.1016/0012-821X(94)00263-X.
- A. Stracke. Earth's heterogeneous mantle: A product of convection-driven interaction between crust and mantle. *Chemical Geology*, 330–331:274–299, 2012. doi: 10.1016/j.chemgeo.2012.08.007.
- A. Stracke and B. Bourdon. The importance of melt extraction for tracing mantle heterogeneity. *Geochimica et Cosmochimica Acta*, 73:218–238, 2009. doi: 10.1016/j.gca.2008.10.015.
- A. Stracke, M. Bizimis, and V. J. M. Salters. Recycling oceanic crust: quantitative constraints. *Geochemistry, Geophysics, Geosystems*, 4, 2003. doi: 10.1029/2001GC000223.
- A. Stracke, A. W. Hofmann, and S. R. Hart. FOZO, HIMU, and the rest of the mantle zoo. *Geochemistry, Geophysics, Geosystems*, 6, 2005. doi: 10.1029/2004GC000824.
- C. Sun and Y. Liang. Distribution of REE between clinopyroxene and basaltic melt along a mantle adiabat: effects of major element composition, water, and temperature. *Contributions to Mineralogy and Petrology*, 163:807–823, 2–12. doi: 10.1007/s00410-011-0700-x.
- S.-s. Sun and W. F. McDonough. Chemical and isotopic systematics of oceanic basalts: implications for mantle composition and processes. *Geological Society, London, Special Publications*, 42: 313–345, 1989. doi: 10.1144/GSL.SP.1989.042.01.19.
- F.-G. Teng, J. Watkins, and N. Dauphas, editors. *Non-traditional stable isotopes*, volume 82 of *Reviews in Mineralogy and Geochemistry*, 2017.

- M. Uchimizu. Geology and petrology of alkali rocks from Dogo, Oki Islands. *Journal of the Faculty of Science, University of Tokyo, Section 2*, 16:85–159, 1966.
- R. Vannucci, B. Bottazzi, E. Wulff-Pedersen, and E.-R. Nuemann. Partitioning of REE, Y, Sr, Zr and Ti between clinopyroxene and silicate melts in the mantle under La Palma (Canary Islands): implications for the nature of the metasomatic agents. *Earth and Planetary Science Letters*, 158:39–51, 1998. doi: 10.1016/S0012-821X(98)00040-5.
- Z. Wang and J. M. Eiler. Insights into the origin of low- $\delta^{18}\text{O}$  basaltic magmas in Hawaii revealed from in situ measurements of oxygen isotope compositions of olivines. *Earth and Planetary Science Letters*, 269:377–387, 2008. doi: 10.1016/j.epsl.2008.02.018.
- Z. Wang, M. Lazarov, L. K. Steinmann, H. Becker, Z. Zou, and X. Geng. The distribution of lead and thallium in mantle rocks: Insights from the Balmuccia peridotite massif (Italian Alps). *American Mineralogist*, 103:1185–1199, 2018. doi: 10.2138/am-2018-6423.
- L. E. Wasylenki, M. B. Baker, A. J. R. Kent, and E. M. Stolper. Near-solidus melting of the shallow upper mantle: partial melting experiments on depleted peridotite. *Journal of Petrology*, 44: 1163–1191, 2003. doi: 10.1093/petrology/44.7.1163.
- B. L. Weaver. The origin of ocean island basalt end-member compositions: trace element and isotopic constraints. *Earth and Planetary Science Letters*, 104:381–397, 1991. doi: 10.1016/0012-821X(91)90217-6.
- D. Weis and F. A. Frey. Isotope geochemistry of Ninetyeast Ridge basement basalts: Sr, Nd, and Pb evidence for involvement of the Kerguelen hot spot. *Proceedings of the Ocean Drilling Program, Scientific Results*, 121:591–610, 1991. doi: 10.2973/odp.proc.sr.121.170.1991.
- W. B. White. Probing the Earth's deep interior through geochemistry. *Geochemical Perspectives*, 4:95–251, 2015.
- M. Willbold and A. Stracke. Trace element composition of mantle end-members: Implications for recycling of oceanic and upper and lower continental crust. *Geochemistry, Geophysics, Geosystems*, 7, 2006. doi: 10.1029/2005GC001005.
- M. Willbold and A. Stracke. Formation of enriched mantle components by recycling of upper and lower continental crust. *Chemical Geology*, 276:188–197, 2010. doi: 10.1016/j.chemgeo.2010.06.005.
- B. J. Wood and E. S. Kiseeva. Trace element partitioning into sulfide: how lithophile elements become chalcophile and vice versa. *American Mineralogist*, 100:2371–2379, 2015. doi: 10.2138/am-2015-5358CCBYNCND.
- B. J. Wood and R. Trigila. Experimental determination of aluminous clinopyroxene-melt partition coefficients for potassic liquids, with application to the evolution of the Roman province potassic magmas. *Chemical Geology*, 172:213–223, 2001. doi: 10.1016/S0009-2541(00)00259-X.

- R. K. Workman and S. R. Hart. Major and trace element composition of the depleted MORB mantle (DMM). *Earth and Planetary Science Letters*, 231:53–72, 2005. doi: 10.1016/j.epsl.2004.12.005.
- R. K. Workman, S. R. Hart, M. G. Jackson, M. Regelous, K. A. Farely, J. Blusztajn, M. Kurz, and H. Staudigel. Recycled metasomatized lithosphere as the origin of the enriched mantle II (EM2) end-member: evidence from the Samoan volcanic chain. *Geochemistry, Geophysics, Geosystems*, 5, 2004. doi: 10.1029/2003GC000623.
- S. Yang, M. Humayun, and V. J. M. Salters. Elemental systematics in MORB glasses from the Mid-Atlantic Ridge. *Geochemistry, Geophysics, Geosystems*, 19:4236–4259, 2018. doi: 10.1029/2018GC007593.
- D. York, N. M. Evensen, M. L. Martinez, and J. D. B. Delgado. Unified equations for the slope, intercept, and standard errors of the best straight line. *American Journal of Physics*, 72:367–375, 2004. doi: 10.1119/1.1632486.
- A. Zindler and S. R. Hart. Chemical geodynamics. *Annual Reviews of Earth and Planetary Science*, 14:493–571, 1986. doi: 10.1146/annurev.ea.14.050186.002425.
- E. Zuleger, J. C. Alt, and J. Erzinger. Data report: trace-element geochemistry of the lower sheeted dike complex, Hole 504B, Leg 140. *Proceedings of the Ocean Drilling Program, Scientific Results*, 148:455–466, 1996. doi: 10.2973/odp.proc.sr.148.112.1996.

## Supplementary material

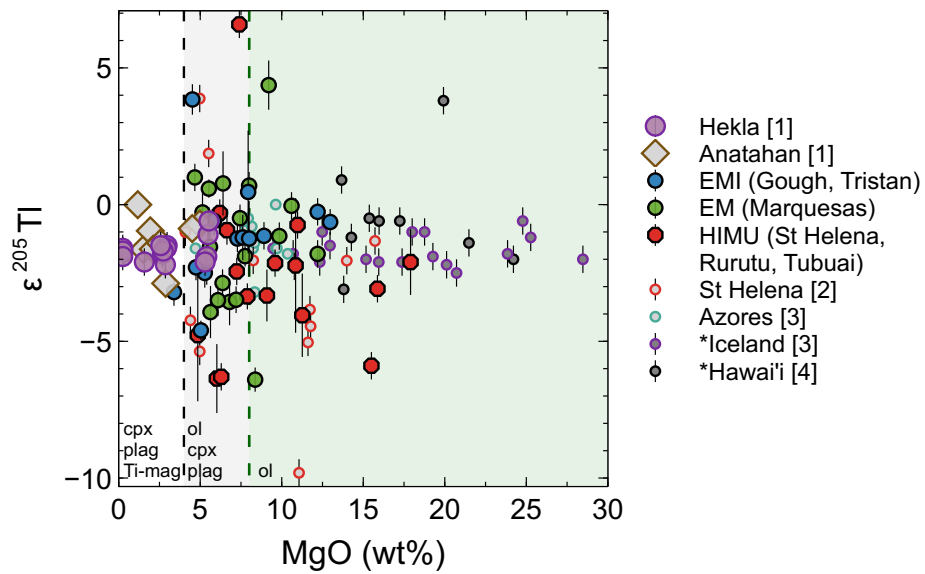


Figure S1: Plot of  $\epsilon^{205}\text{Tl}$  against MgO content of the samples of this study and from the literature.  $\epsilon^{205}\text{Tl}$  does not vary systematically with melt evolution. As the majority of samples are not cogenetic, two suites of lavas following common liquid lines of descent (Hekla, Iceland; Anatahan, Marianas; Prytulak et al., 2017) are highlighted, showing that even at low MgO there is no correlation with  $\epsilon^{205}\text{Tl}$ . Approximate fields of fractionating phases are indicated. Symbols and data sources as in Figure 4, except: [1] Prytulak et al. (2017), [2] Nielsen et al. (2007).

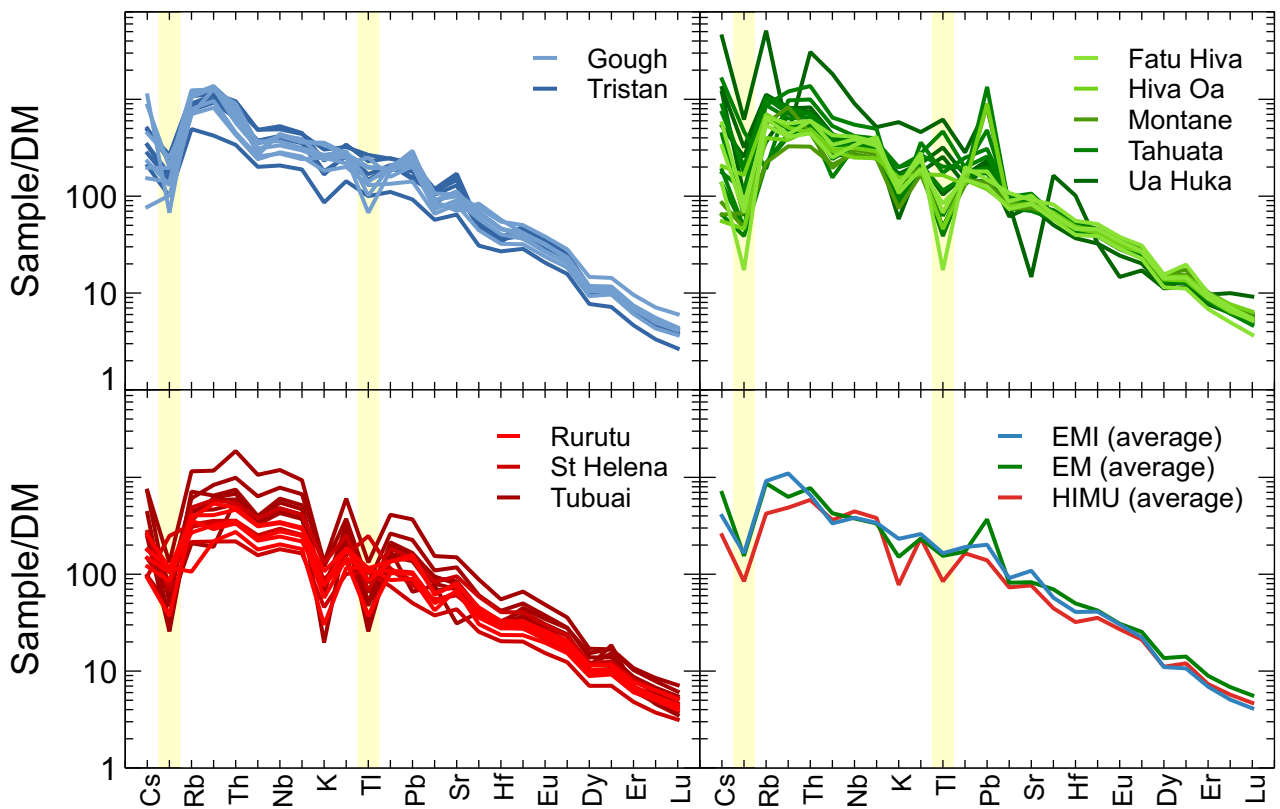


Figure S2: Depleted Mantle-normalised trace element plots. Here the negative Ti anomaly, while still present on average, is less pronounced - particularly for EM-type lavas.

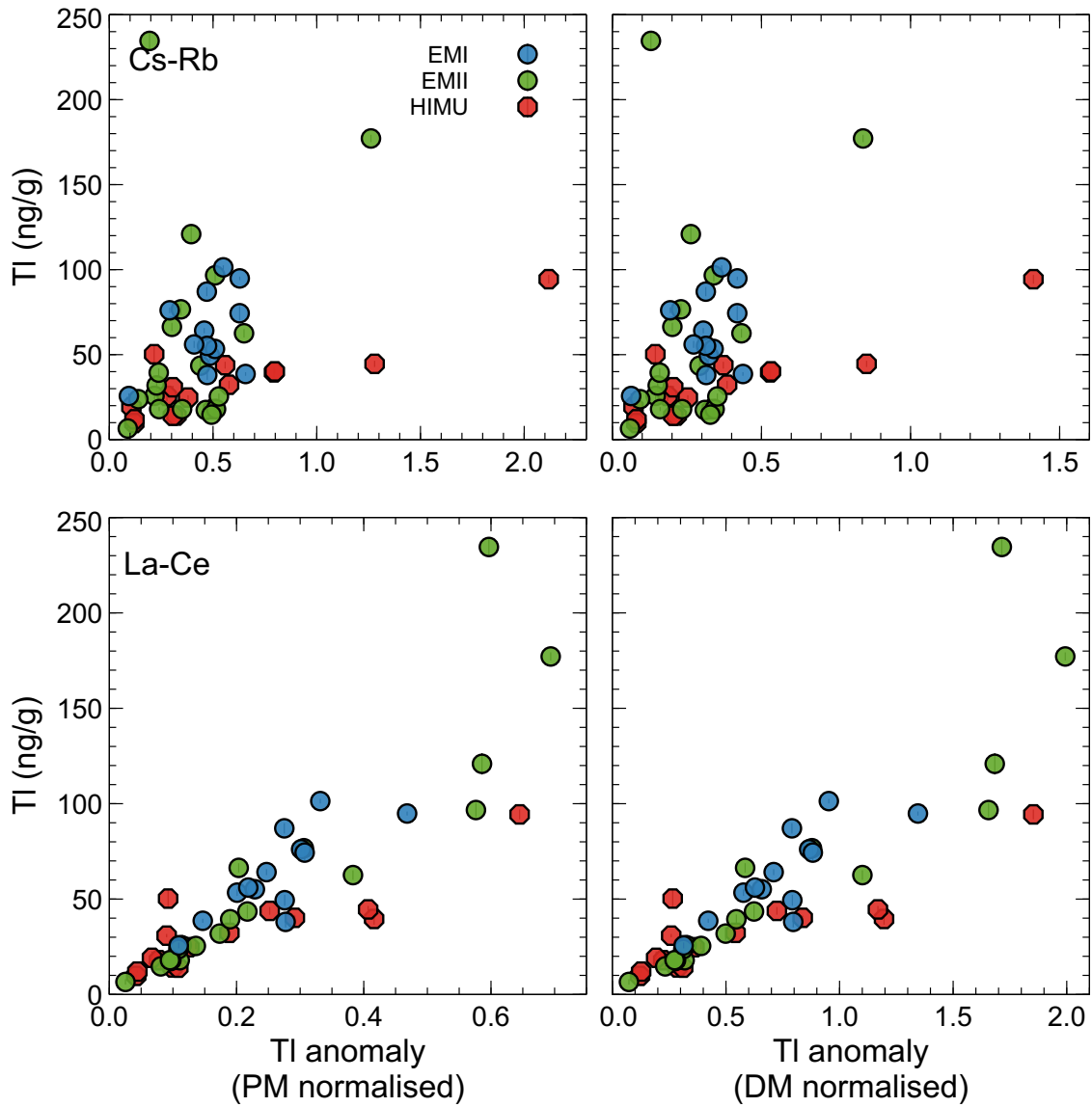


Figure S3: Tl anomaly exhibits clearer covariation with absolute Tl abundance when calculated relative to REE than when calculated relative to LILE (with the possible exception of HIMU). Symbols and data sources as in Figure 4.

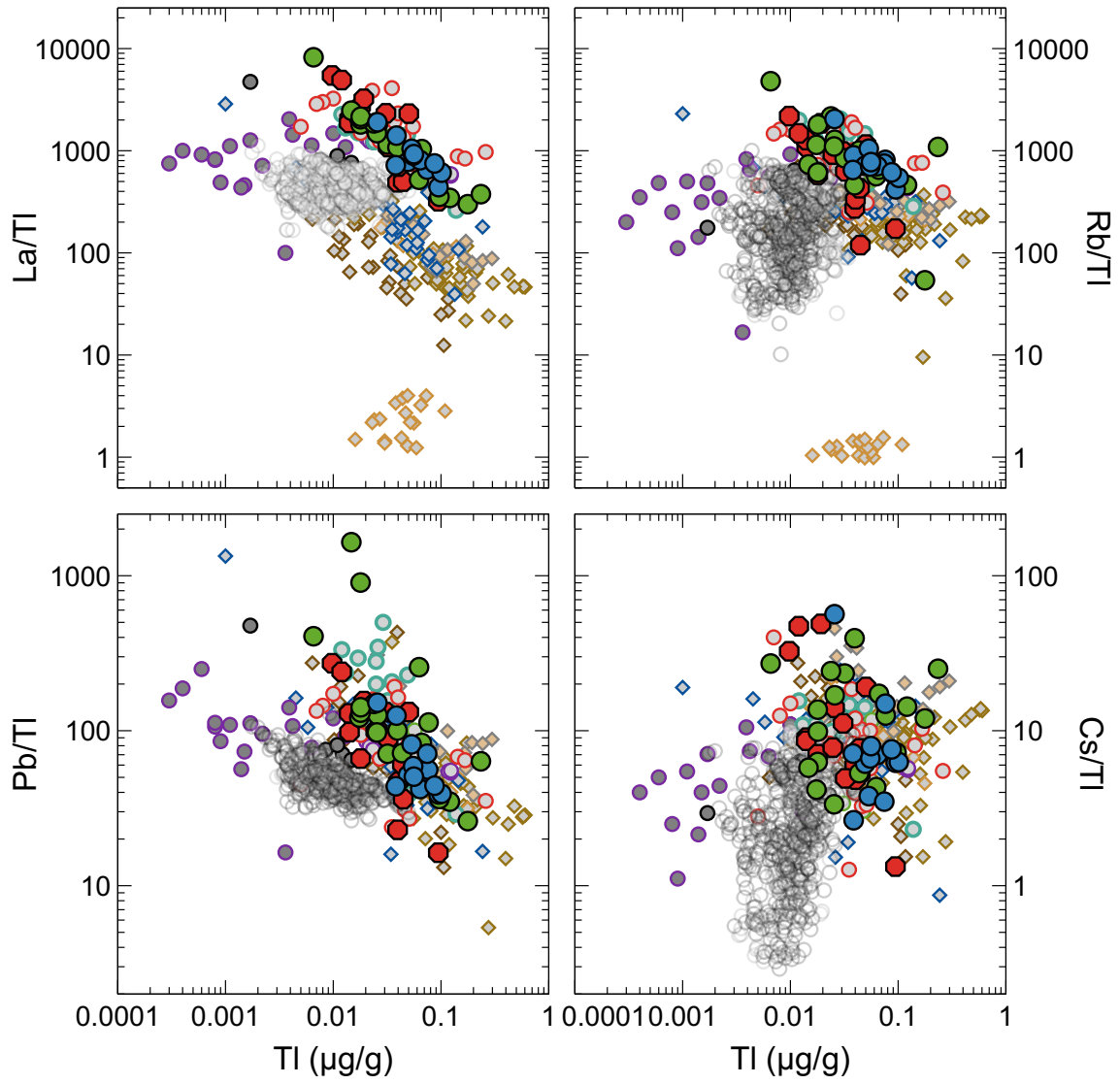


Figure S4: Plot of La/TI, Pb/TI, Rb/TI and Cs/TI ratios against Tl concentration. Only the La/TI ratios distinguishes tectonic settings as clearly as the Ce/TI ratios. Symbols and data sources as in Figure 4.

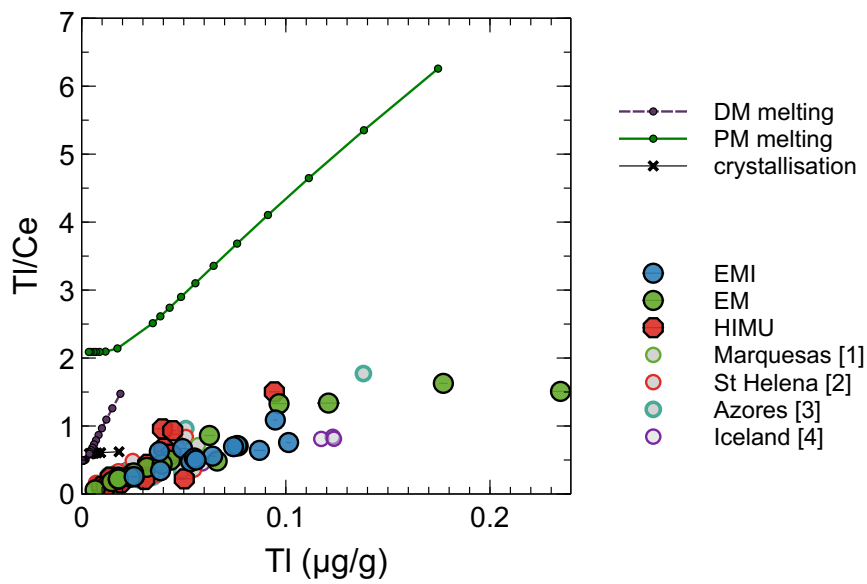


Figure S5: Process identification plot (Minster and Allègre, 1978) of Tl/Ce against  $1/Tl$ . Also shown are melting patterns (melt fraction  $F = 0.0001$  to  $1$ ) for DM ( $Tl = 0.00038 \mu\text{g/g}$ ,  $Ce = 0.772 \mu\text{g/g}$ ) and PM ( $Tl = 0.0035 \mu\text{g/g}$ ,  $Ce = 1.675 \mu\text{g/g}$ ), in addition to the fractional crystallisation trend ( $F = 1$  to  $0.1$ ), assuming bulk  $D^{Tl} = 0.02$  and bulk  $D^{Ce} = 0.06$ . While most of the variation in OIB is subparallel to the DM melting trend, with scatter leaving room for some fractional crystallisation, the observed range significantly exceeds that which can be explained simply through a combination of melting and fractional crystallisation. The OIB trend therefore requires mixing melts from different sources, one of which cannot contain more than negligible Tl (note y-intercept of trend). Large symbols: this study. Other data sources: [1] Chauvel et al. (2012); [2] Blusztajn et al. (2018); [3] Nielsen et al. (2007); [4] Prytulak et al. (2017).

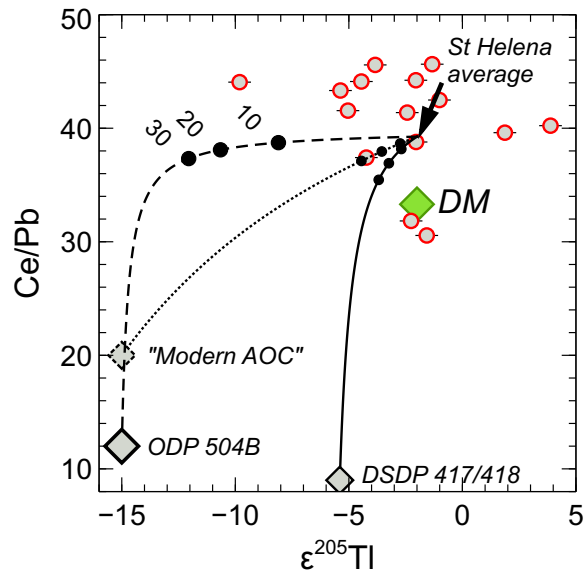


Figure S6: Mixing between St Helena HIMU average composition (Blusztajn et al., 2018) and three "AOC" values (see Table S1). Ticks correspond to admixture of 10%, 20% and 30% of AOC as labelled for ODP 504B.

Table S1: For DM, values are taken from Salters and Stracke (2004), except  $\epsilon^{205}\text{Tl}$  (Nielsen et al., 2006b). For DSDP 417/418, supercomposite values are taken from Blusztajn et al. (2018) and Staudigel et al. (1995). ODP 504B values are taken from Nielsen et al. (2006c) and Bach et al. (2003). "Modern AOC" values are taken from Blusztajn et al. (2018) or inferred (underlined). St Helena average values are as reported by Blusztajn et al. (2018).

	DM	St Helena average	ODP 504B (~6.6 Ma)	DSDP 417/418 (~109 Ma)	"Modern AOC"
Tl ( $\mu\text{g/g}$ )	0.00038	0.03	0.25	0.07	<u>0.017</u>
Ce ( $\mu\text{g/g}$ )	0.772	80.83	4.31	6.19	<u>12</u>
Pb ( $\mu\text{g/g}$ )	0.0232	2.06	0.36	0.69	<u>0.6</u>
Ce/Pb	33	~40	12	9	20
$\epsilon^{205}\text{Tl}$	-2	~-2	-15	-5.4	-15